Department of Chemistry
Faculty of Science
University of Helsinki

INORGANIC NANOSTRUCTURES PREPARED BY ELECTROSPINNING AND ATOMIC LAYER DEPOSITION

Eero Santala

DOCTORAL DISSERTATION

To be presented for public discussion with the permission of the Faculty of Science of the University of Helsinki, in Auditorium A110, Chemicum, on the 10th of January 2020 at 12 o'clock.

Helsinki 2020

Supervisor

Professor Mikko Ritala
Department of Chemistry
Faculty of Science
University of Helsinki
Finland

Reviewers

Professor Gregory N. Parsons
Department of Chemical and Biomolecular Engineering
North Carolina State University
USA

Professor Mika Suvanto
Department of Chemistry
University of Eastern Finland
Finland

Opponent

Professor Erkki Levänen
Materials Science and Environmental Engineering
Faculty of Engineering and Natural Sciences
Tampere University
Finland

ISBN 978-951-51-5678-5 (paperback)
ISBN 978-951-51-5679-2 (PDF)
http://ethesis.helsinki.fi

Unigrafia
Helsinki 2020

”There and Back Again"
J. R. R. Tolkien

ABSTRACT

Nanostructures are structures where at least one dimension is in nanoscale which ranges typically from 1 to 100 nm. 1D nanostructure is an object where two dimensions are in the nanometer scale and one dimension in a larger scale, for example carbon nanotubes and electrospun fibers. Due to a very small size, nanostructured materials have different properties than what they have in bulk form, for example chemical reactivity is increased when the size comes smaller.

Electrospinning is a very simple but versatile and scalable method for preparing micro- and nanosized fibers. In an electrospinning process an electrical charge is used to spin very fine fibers from a polymer solution or melt. By changing electrospinning parameters, for example voltage and spinneret-collector distance, fibers of different diameters can be obtained. With different electrospinning setups it is also possible to prepare hollow fibers, and even macroscopic objects with fiber walls can be obtained.

This work was concentrated on A) constructing different electrospinning setups and verifying their operation by electrospinning various materials, and B) preparing 1D nanostructures like inorganic nanofibers directly by electrospinning and nanotubes by combining electrospinning and atomic layer deposition, ALD. This is so called Tubes by Fiber Template (TUFT) –process.

The electrospinning setup was constructed successfully, and its operation was verified. Several materials were electrospun. Polymers (PVP, PVA, PVAc, PEO, PMMA and PVB, Chitosan) were electrospun directly from polymer/solvent solution, and ceramic materials like TiO_2, $BaTiO_3$, SnO_2, CuO, IrO_2, ZnO, Fe_2O_3, $NiFe_2O_4$, $CoFe_2O_4$, SiO_2 and Al_2O_3 were electrospun from polymer solutions containing the corresponding metal precursor(s). In the case of the ceramic fibers, the electrospinning was followed by calcination to remove the polymer part of the fibers. Metallic fibers were obtained by a reduction treatment of the corresponding oxides, for example Ir fibers were prepared by reducing IrO_2 fibers.

Combination of electrospinning and ALD was used for TUFT processing of ceramic nanotubes. In the TUFT process, electrospun template fibers were coated with the desired material (Al_2O_3, TiO_2, IrO_2, Ir, PtO_x and Pt) and after coating the template fibers were removed by calcination. The inner diameter of the resulting tubes was determined by the template fiber and the tube wall thickness by the thickness of the ALD deposited film.

Promising results were obtained in searching for new applications for electrospun fibers. For the first time, by combining electrospinning and ALD, the TUFT process was used to prepare reusable magnetic photocatalyst fibers. These fibers have a magnetic core fiber and a photocatalytic shell around it. After a photocatalyst purification was completed, the fibers could be collected from the solution by a strong magnet and reused in cleaning the next solution.

In this study, the most commercially and environmentally valuable application invented was to use electrospun ion selective sodium titanate nanofibers for purification of radioactive wastewater. These fibers were found to be more efficient than commercial granular products, and they need much less space in final disposal.

PREFACE

This dissertation is based on experimental work carried out during the years 2004-2017 in the Laboratory of Inorganic Chemistry at the University of Helsinki. The work was supported financially by the Academy of Finland (Finnish Centre of Excellence in Atomic Layer Deposition) and the former Finnish Funding Agency for Technology and Innovation (TEKES).

I am most grateful to Professors Mikko Ritala and Markku Leskelä for invitation and giving me an opportunity to be a part of your ALD group. It has been a privilege to learn a little bit of that huge knowledge that you both have. Especially I want to thank my supervisor Professor Mikko Ritala for patience, support and kind guidance with my research.

I would also like to thank the reviewers of this dissertation, Professors Gregory Parsons and Mika Suvanto, for their comments regarding my work.

Thanks to my closest co-worker, co-author and roommate Jani Holopainen. The purpose was to teach you everything about the electrospinning. I think I succeeded because suddenly the master became a student. I truly believe, that in this case we both are winners.

Thanks also to all other co-authors, Mikko Heikkilä for helping me in XRD and XRR measurements, Marianne Kemell for teaching me in using of FESEM and EDS, Jani Hämäläinen for helping me with ALD reactors, Jun Lu for making all TEM-imaging for my papers, and Risto Koivula for advising me in radiochemistry. It was a pleasure that you all helped me along this journey.

During these 14 years I had quite many roommates, I want to thank you all. Thanks also to all other colleagues in Laboratory of Inorganic chemistry, thanks for those interesting discussions in the coffee room. Despite my bad jokes we had many joyful moments.

I'm also very grateful to Eila Hämäläinen, my chemistry teacher from the Hollola High School. Without your inspirational teaching and thoughts, I probably would never have started to study chemistry.

Thanks also to my friends from Hollola, friends from Vacappella, friends from Chamber Choir of Vantaa and all colleagues from the Football Club of Nurmijärvi, NJS. You all have brought to my life so much content from outside the scientific world.

The big thanks also to my mother Hilkka, father Jouko and all three sisters Elina, Marika and Taija for all the support they have given me over the years.

Last, I want to thank my own family, my sons Eetu and Eppu, daughter Elli and dog Siru but especially my wife Maari for her patience and love. You all are the most important thing in my life.

This dissertation is dedicated to the memory of my father.

Nurmijärvi, January 2020

Eero Santala

CONTENTS

LIST OF ORIGINAL PUBLICATIONS

This thesis is based on the following publications:

I **Exploitation of atomic layer deposition for nanostructured materials**
M. Leskelä, M. Kemell, K. Kukli, V. Pore, E. Santala, M. Ritala and J. Lu
Mater. Sci. Eng. C 27 (**2007**) 1504-1508.

II **The preparation of reusable magnetic and photocatalytic composite nanofibers by electrospinning and atomic layer deposition**
E. Santala, M. Kemell, M. Leskelä, M. Ritala
Nanotechnology 20 (**2009**) 035602.

III **Metallic Ir, IrO_2 and Pt nanotubes and fibers by electrospinning and ALD**
E. Santala, J. Hämäläinen, J. Lu, M. Leskelä and M. Ritala
Nanosci. Nanotechnol. Lett. 1 (**2009**) 218–223.

IV **Needleless electrospinning with twisted wire spinneret**
J. Holopainen, T. Penttinen, E. Santala and M. Ritala
Nanotechnology 26 (**2015**) 025301.

V **Electrospun sodium titanate fibers for fast and selective water purification**
E. Santala, R. Koivula, R. Harjula and M. Ritala
Environ. Technol. 40 (**2019**) 3561-3567.

The publications are referred to in the text by their roman numerals.

OTHER PUBLICATIONS BY THE AUTHOR

1. **Selective-area atomic layer deposition using poly(vinyl pyrrolidone) as a passivation layer.**
E. Färm, M. Kemell, E. Santala, M. Ritala and M. Leskelä
J. Electrochem. Soc. 157 (**2010**), K10-K14.

2. **Thermal study on electrospun polyvinylpyrrolidone / ammonium metatungtate nanofibers: Optimising the annealing conditions for obtaining WO_3 nanofibers**
I. M. Szilágyi, E. Santala, M. Heikkilä, M. Kemell, T. Nikitin, L. Khriachtchev, M. Räsänen, M. Ritala and M. Leskelä
J. Therm. Anal. Calorim. 105(1) (**2011**), 73-81.

3. **Controlling the crystallinity and roughness of atomic layer deposited titanium dioxide films**
R. L. Puurunen, T. Sajavaara, E. Santala, V. Miikkulainen, T. Saukkonen, M. Laitinen and M. Leskelä
J. Nanosci. Nanotechnol. 11(9) (**2011**), 8101-8107.

4. **Reducing stiction in microelectromechanical systems by nanometer-scale films grown by atomic layer deposition**
R. L. Puurunen, A. Häärä, H. Ritala, J. Dekker, H. Pohjonen, T. Suni, J. Kiihamäki, E. Santala, M. Leskelä and H. Kattelus
Sens. Actuators, A 188 (**2012**), 240-245.

5. **Photocatalytic properties of WO_3/TiO_2 core/shell nanofibers prepared by electrospinning and atomic layer deposition**
I. M. Szilagyi, E. Santala, M. Heikkilä, V. Pore, M. Kemell, T. Nikitin, G. Teucher, T. Firkala, L. Khriachtchev, M. Räsänen, M. Ritala and M. Leskelä
Chem. Vap. Deposition 19(4-5-6) (**2013**), 149-155.

6. **Low-temperature magnetism of alabandite: crucial role of surface oxidation**
J. Čuda, T. Kohout, J. Filip, J. Tuček, A. Kosterov, J. Haloda, R. Skála, E. Santala, I. Medřík and R. Zbořil
Am. Mineral. 98(8-9) (**2013**), 1550-1556.

7. **Preparation and bioactive properties of nanocrystalline hydroxyapatite thin films obtained by conversion of atomic layer deposited calcium carbonate**
J. Holopainen, K. Kauppinen, M. Kenichiro, E. Santala, E. Mikkola, M Heikkilä, H. Kokkonen, M. Leskelä, P. Lehenkari, J. Tuukkanen and M. Ritala
Biointerphases 9(3) (**2014**), 031008/1-031008/10.

8. **Electrospinning of calcium carbonate fibers and their conversion to nanocrystalline hydroxyapatite**
J. Holopainen, E. Santala, M Heikkilä and M. Ritala
Mater. Sci. Eng. C. 45 (**2014**), 469-476.

9. **Osteoclasts in the interface with electrospun hydroxyapatite**
J. Pasuri, J. Holopainen, H. Kokkonen, M. Persson, K. Kauppinen, P. Lehenkari, E. Santala, M. Ritala and J. Tuukkanen
Colloids Surf. B. 135 (**2015**), 774-783.

10. **Metamaterial thin films**
O. J. Glembocki, S. M. Prokes, J. D. Caldwell, M. Ritala, M. Leskelä, J. Niinistö, E. Santala, T. Hatanpää, and M. Kariemi
U. S. Patent 9878516 (B2) (**2018**).

11. **Novel ion exchange materials**
R. Harjula, R. Koivula, M. Ritala, E. Santala, J. Holopainen, and E. Tusa
Finnish Patent 127747 B (**2019**).

ABBREVIATIONS

ac	acetate
acac	acetylacetonate
ALD	atomic layer deposition
CVD	chemical vapor deposition
DCM	dichloromethane
DMF	dimethylformamide
EB	electroblowing
EL	electroluminescence
EtOH	ethanol
FESEM	field emission scanning electron microscope
FR	feed rate
MB	methylene blue
M_w	molecular weight
NTWE	needleless twisted wire electrospinning
^{i}PrOH	isopropanol
ITO	indium tin oxide
PEO	poly(ethylene oxide)
PMMA	poly(methyl methacrylate)
PU	polyurea
PVA	poly(vinyl alcohol)
PVAc	poly(vinyl acetate)
PVB	poly(vinyl butyral)
PVP	poly(vinyl pyrrolidone)
SAED	selected area electron diffraction
SEM	scanning electron microscope
STEM	scanning transmission electron microscope
TFA	trifluoroacetic acid
TGA	thermogravimetric analysis
TMA	trimethylaluminum
TEOS	tetraethoxysilane
TUFT	tubes by fiber templates
UV-light	ultraviolet light
V_c	critical voltage
XRD	x-ray diffraction
XRR	x-ray reflectance

1 INTRODUCTION

Nanostructured materials are an interesting and increasingly studied topic. Due to the very small size, materials in the nanoscale may have different properties than what they have in the bulk form. For example, bulk TiO_2 like the common pigment grade TiO_2 consist of large enough crystals to scatter visible light and appears therefore white. In TiO_2 thin films and nano sized TiO_2 used in sun lotions the particles are so small compared to visible wavelengths that they do not scatter visible light. In all forms TiO_2 absorbs ultraviolet light, however, because its band-gap energy (rutile: 3.0 eV, anatase: 3.2 eV) matches well with the onset of the UV region (wavelengths < 400 nm, energy > 3.10 eV) and therefore TiO_2 is used extensively for UV-protection and photocatalysis. Also, other properties of materials can vary, for example chemical reactivity is increased when the size is smaller, because the fraction of surface atoms is increased.

The word **nano** is coming from Greek word '*nanos*' (*νάνος*), which means '*dwarf*'. In science, '*nano*' is a prefix meaning 10^{-9}, for example a nanometer is one billionth of a meter.[1] For comparison, an atom radius is from about 0.03 to 0.26 nm.[2] When speaking of an atom radius, the common unit is ångström [Å], which means 10^{-10} m or 0.1 nm. For example, the radius of a fullerene C_{60} molecule is about 10 Å.

Usually, when speaking about **nanostructures**, we are speaking about structures which have at least one dimension in a nanoscale. The **nanoscale** is a length scale which is usually cited as 1 - 100 nanometers. Nanostructures can be divided to four categories: 3D, 2D, 1D and 0D (Figure 1).[3]

3D structures: all three dimensions are in the macroscopic scale, but the material is composed of other nanostructures (2D, 1D and 0D) forming a porous object.

2D structures: only one dimension is in the nanoscale, and the other two dimensions are in the macroscopic scale, for example, thin films.

1D structures: two dimensions are in the nanoscale and only one in the macroscopic scale, for example carbon nanotubes and electrospun nanofibers.

0D structures: all three dimensions are in the nanoscale, for example nanoparticles and quantum dots.

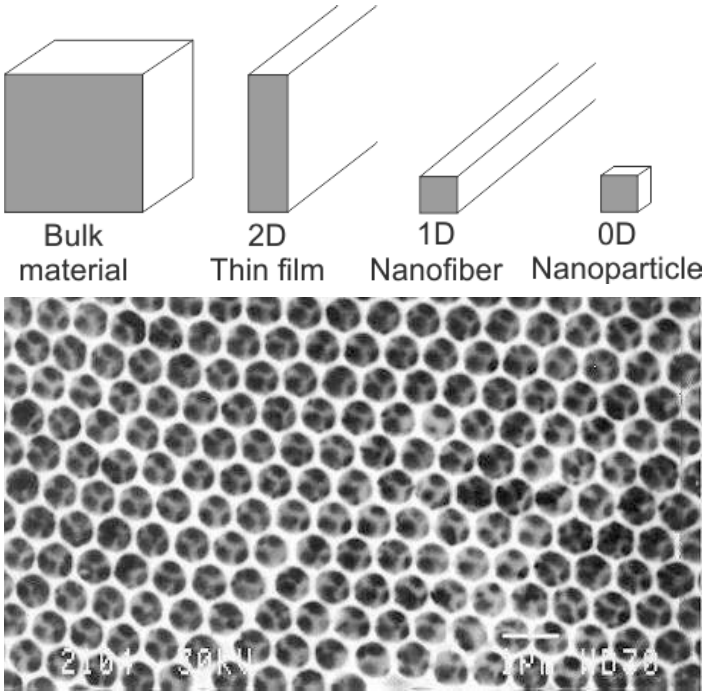

Figure 1 (Top) Bulk material and structures confined structures in 2, 1 and 0 dimensions and (Bottom) in 3 dimensions. Bottom Figure reprinted from [3] by permission of Springer Nature, Copyright (1999).

These four (3D, 2D, 1D and 0D) structure categories are only the simplest nanostructure types, and often in real world combinations of these four types are found in nanostructures.

Nanoscience is a multidisciplinary science which combines chemistry, physics, biology and medicine together.[4] Nanoscience is investigating basic phenomena in the nanoscale and properties of nanostructures. For example, reactive surface area in nanopowder is much higher than in the same mass of bulk material. The higher surface area means that nanoparticles have relatively more surface atoms than larger particles because when the diameter of a particle is decreasing the fraction of surface atoms is increasing. The higher surface area can lead to higher reactivity in chemical reactions. Nanoscience is often investigating how a certain nanostructure can be made and what are its properties.

Nanotechnology is studying how nanoscience and its results can be benefitted in new applications, and how to improve existing applications by using nanostructures. Nanotechnology is also investigating how a certain nanostructure can be made. [4] It can be thought that nanotechnology is driven by financial interests while the nanoscience is driven by pure scientific curiosity.

In this study we have concentrated on preparing inorganic nanostructures by using an electrospinning method only, or by combining it with an ALD (atomic layer deposition) method. We have developed a new way to perform the TUFT (Tubes by Fiber Template) process[5] (Figure 2a) to make nanotubes by depositing an ALD coating on electrospun fibers and then removing the fiber template.[I, III]

We have also developed a new TUFT route to prepare particle loaded tubes (Figure 2c), where photocatalytic TiO_2 tubes with magnetic core were made by electrospinning the magnetic core fiber and coating it with ALD TiO_2 thin film.[II] Also new electrospinning processes were developed to make new materials like Ir/IrO_2 or Pt/PtO_x fibers and nanotubes.[III] We have also prepared, for the first time ever, inorganic metal oxide ion exchange fibers by using electrospinning.[V] Finally we also have developed a novel Needleless Twisted Wire Electrospinning setup (Figure 3) which increases production rate significantly compared to the conventional single needle system.[IV]

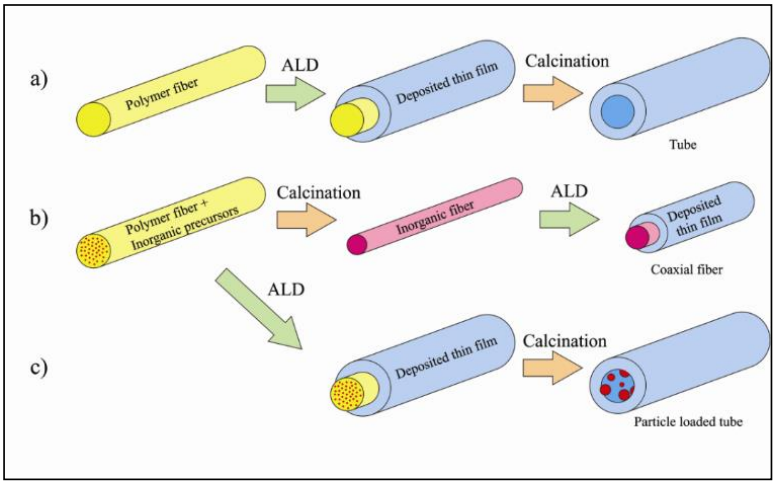

Figure 2 Schematic picture how to combine electrospinning and ALD to prepare different types of nanostructures. Reprinted from [II] by permission of IOP Publishing, Copyright (2009).

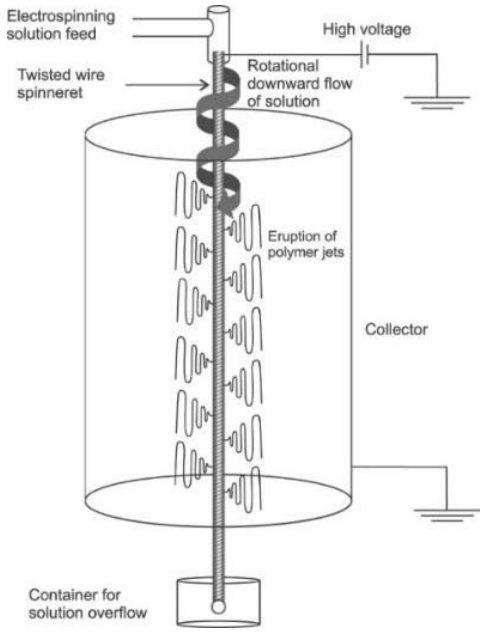

Figure 3 Schematics of Needleless Twisted Wire Spinneret system. Reprinted from [IV] by permission of IOP Publishing, Copyright (2015).

2 ELECTROSPINNING

An **electrospinning** process, also known as an electrostatic spinning, was patented by Anton Formhals in 1934.[6] The patent describes how polymer fibers are made by using electrostatic force. In the electrospinning process a polymer solution or melt is spun to nanofibers by an electrically charged jet. During the last two decades electrospinning processes, materials and applications have been studied extensively by many groups, like Reneker et al.,[7-9] Greiner & Wendorff et al.,[5,10,11] Li et al.[12-21] and Ramakrishna et al.[22-27] This development has been affected by advances in electron microscopy and growing interest in nanotechnology.

2.1 Apparatus

The electrospinning apparatus can be very simple.[17,26] It may consist only of a container (1), for example a pipette or a plastic syringe with a metallic needle, which is connected to a high voltage power supply (2), and a collector (3) like an electrically grounded metal plate (Figure 4). There can also be additional supplies, like a syringe pump to control the flow rate of the polymer solution. The collector or part of it can be set at a counter voltage with another high voltage power supply. The collector can be motion-controllable, and its shape affects how fibers are aligned on its surface.

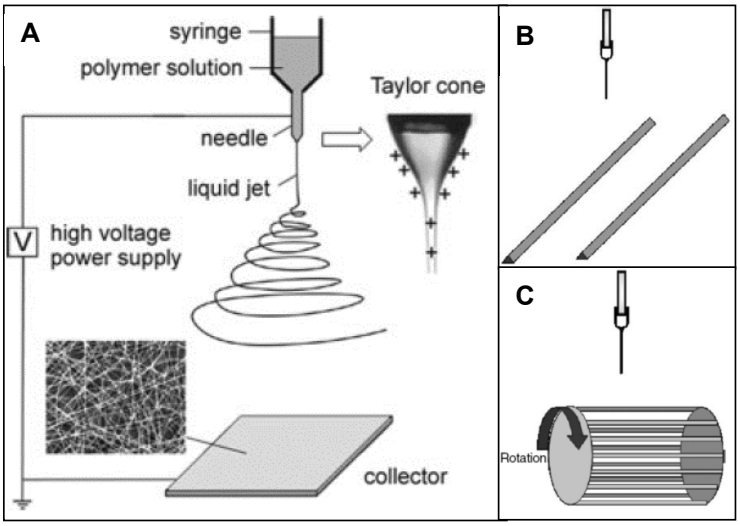

Figure 4 A) A typical electrospinning set-up using a grounded static collector and some examples of different types of collectors: B) parallel electrodes and C) a rotating wire drum collector. Figure A reprinted from [17] by permission of John Wiley and Sons, Copyright (2004). Figure B and C reprinted from [26] by permission of IOP Publishing, Copyright (2006).

2.2 Electrospinning process

In a simplified electrospinning process,[17,22] a high voltage is applied through a metallic needle to a polymer solution which is placed for example into a plastic syringe. The polymer solution in the syringe is charged, electrostatic repulsion overcomes the surface tension and a droplet is stretched at the needle tip. When the electric charge in the polymer solution reaches a critical amount, the polymer droplet forms a Taylor cone (Figure 4).[28] A jet of the polymer solution is emitted from the Taylor cone and travels towards a lower electrical potential, which is usually the electrically grounded collector.

Reneker et al.[7,8] noted that the travel from the Taylor cone to the collector can be divided to two parts. In the first part, which starts from the Taylor cone and is so called straight jet region, the jet path is straight and no stretching and thinning of the fiber occurs. In the second and last part of the jet, the jet begins to whip as caused by electrostatic repulsions at small bends. This second part of the jet is also called instable region. The jet is flailing until it reaches the grounded collector. Only in the instable region the jet comes thinner and forms a uniform and submicrometer or nanometer-scale fiber.

During the way from the tip to the collector, the solvent evaporates, and the jet forms a polymer fiber and that comes thinner until it is completely dried out of the solvent or reaches the collector. While this is the simplest way to describe the electrospinning process, there are several parameters which influence the electrospinning process and the morphology of the final product. These parameters can be divided to the solution parameters, processing parameters, and ambient conditions or parameters. When all these parameters and their effects are known and well understood, it is possible to make different setups of the electrospinning apparatus and to prepare several forms and arrangements of fibrous structures.

2.2.1 Solution parameters

Polymer solution parameters such as **viscosity**, **surface-tension**, **conductivity**, and **dielectric constant of the solvent** have the most significant influence on the electrospinning process and morphology of the final product. These parameters have a major effect on the fiber formation and the uniformity of the final fiber. Table 1 shows how these properties of the solution affect the electrospinning process and how to make improvements to get a better final product.

Table 1. *Solution parameters that have an effect to the electrospinning process.*

Parameter	If	Result	How to adjust
Viscosity	too low [29]	spray	by polymer molecular weight or by concentration
	low [30,31]	beads in fibers	
	increasing [32]	smaller deposition area	
	too high [33,34]	difficulties to get solution out from the needle	
Surface tension	too high [30,35]	beads in fibers or spray	by proper solvent or surfactant
Conductivity of solution	increased [34,36]	smoother fibers	by adding salts or by adjusting pH
		less beads in fibers	
		larger deposition area	
		thinner fibers	
Dielectric constant of a solvent	higher [37,38]	less beads	by solvent selection
		thinner fibers	

Viscosity

Viscosity is a measure of the flowing resistance of a fluid which is being deformed. In the spoken language, viscosity can be understood as a "thickness" of a fluid or friction at the molecular level. A polymer solution of a high molecular weight polymer has higher viscosity than a polymer solution of the same polymer with a lower molecular weight. The viscosity of the solution can thus be adjusted by varying / selecting the molecular weight of the polymer or by changing the concentration of the chosen polymer (Table 1).

Viscosity determines the result of the electrospinning process. When viscosity is too low, the process is electrospray and no fibers are formed.[29] By increasing the viscosity, the result is changed to fibers with beads,[30,31] or smoother fibers[32] (Figure 5). Changing the viscosity also affects the deposition area of the fibers on the collector. Increasing the viscosity makes the solution “thicker” and leads to a smaller deposition area.[32] When the viscosity is increased too high it becomes difficult to get the solution out from the needle.[33,34]

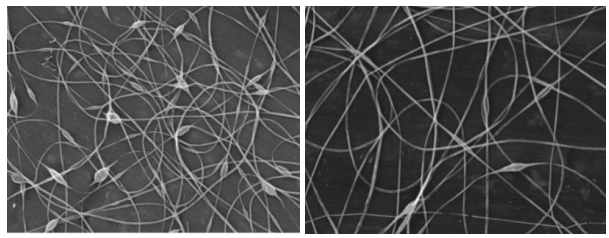

Figure 5 Effect of poly (ethylene oxide) solution viscosity on the morphology of beaded fibers. Viscosity of the polymer solution was (Left) 160 cP and (Right) 527 cP. Reprinted from [30] by permission of Elsevier, Copyright (1999).

Surface tension

Surface tension of the polymer solution is also an important parameter in the electrospinning process (Table 1). Successful electrospinning requires that the electrostatic repulsion caused by the applied voltage overcomes the surface tension. Too high surface tension of the polymer solution may also cause formation of beads along the jet. Surface tension can be adjusted to the right level by choosing a proper solvent or a solvent mixture, or by adding some surfactant to the solution.[30,35]

Conductivity of solution

The electrospinning process occurs when a critical voltage is achieved and charges in the polymer solution overcome the surface tension. When conductivity of the solution is increased, also its charging capability is increased. Conductivity can be increased by adding to the polymer solution some inert ions or salt or by adjusting the pH (Table 1).[36] By increasing charged species and conductivity, the critical voltage comes lower and stretching of the solution is increased. Increased charge in the polymer solution gives greater bending instability, which means that the deposition area is increased, and the resulting fibers will be thinner. Higher stretching induces smoother fibers, decreased formation of beads, and thinner fibers can be obtained.[34]

Dielectric constant of a solvent

Dielectric constant of a solvent has also a role in the electrospinning process (Table 1). Because of the higher dielectric constant the bending instability of the electrospinning jet is increased and at the same time the jet path and deposition area are increased.[38] By using a solvent with a high dielectric constant, formation of the beads is reduced, and the resulting fibers are thinner.[37]

2.2.2 Processing parameters

Processing parameters during the electrospinning process have a certain influence on the fiber morphology. The processing parameters can be divided to various external factors: **voltage**, **feed rate**, **temperature**, effect of **collector**, inner **diameter of needle** and **needle-collector distance** (Table 2).

Table 2. *Processing parameters and their influence on the electrospinning process.*

Parameter	If	Then	Result
Voltage	$V < V_c$ [28]	no Taylor cone	no fiber formation
	$V \geq V_c$ [28]	Taylor cone	fiber formation begins at V_c
	higher V [31,39-42]	faster jet and evaporation	thinner fibers
		shorter flight time and path	thicker fibers
	lower V [42]	longer flight time and path	thinner fibers
Feed rate (FR)	higher FR [34,43]	more solution is coming out from needle	thicker fiber
	too high FR [43]	instable Taylor cone	fiber formation is not stable
		it takes a longer time for the jet to dry	fibers can be fused together
	lower FR [43]	stable Taylor cone	thinner fiber
Temperature	higher [32,44]	higher evaporation rate	thicker fibers
		lower viscosity	more uniform fibers
Needle (inner diameter)	smaller [42]	smaller droplet	thinner fibers
		higher surface tension	needs more charges to initiate the jet
	too small [42]	no droplet	no fibers
Collector	electrically conductive [22]	collector is discharging	fibers collected with higher density
	electrically non-conductive [45]	collector is charging and repulsive forces develop	lower fiber packing density and 3D fiber structures
	shape of (for example, collector cylinder)		different shape of fiber mat [46]
	patterned collector		alignment of fibers [12]
	moving (for example, rotating collector drum)		alignment of fibers [47]
Needle – collector distance	too low [39]	short flight time, not enough time for solvent evaporation	wet or fused fibers
		strong electric field and fast acceleration of the jet	fibers are merged together
	higher [8,42,48]	longer flight time	thinner fibers
		smaller electric field causes less stretching in the jet	thicker fibers
	too high [41]	fibers get deposited somewhere else than on the collector	no fibers on the collector

Voltage

The most important parameter in the electrospinning process is the voltage that is applied to the electrospinning solution in the syringe. The voltage between the needle and the collector makes the electric field and initiates the electrospinning process when the critical voltage (V_c) is achieved and the Taylor cone is formed.[28]

When the voltage is equal or higher than the critical voltage, Taylor cone is formed to the droplet at the tip of the needle.[28] In the polymer solution jet that is erupted from the Taylor cone, the coulombic repulsions stretch the solution to the resulting fibers. If the applied voltage is smaller than the critical voltage, no Taylor cone is formed, and no fibers are obtained. Successful electrospinning process requires that the Taylor cone is stable, and this can be achieved by adjusting the voltage together with the feed rate of the polymer solution.

The process voltage provides the required charge in the solution and it has several effects on the fiber formation (Table 2). First, a higher voltage creates more charge and thereby causes the jet to accelerate faster and forces more solution out of the tip of the needle. The higher the voltage and therefore the bigger the coulombic forces, the more the solution stretches and the fiber becomes thinner.[30,39,40] Higher voltage also accelerates the jet more quickly and thereby encourages faster evaporation that leads to drier fibers.[41] However, as the increased process voltage increases the acceleration of the polymer jet, also the flight time of the jet becomes shorter.[42] This leads to a shorter jet path and the diameter of the resulting fiber is increased. Lower voltage gives longer flight time and the jet has more time to stretch and elongate. The optimization of the voltage, together with the other process parameters, must be done case by case, keeping in mind what the product should be in the end.

Feed rate

After the process voltage the next important process parameter is the feed rate or flow rate of the solution (Table 2). The feed rate determines the volume of the solution flows through the tip of the electrospinning needle.

When the feed rate is increased more solution comes out from the needle tip, and if at the same time the voltage is kept constant, the result is thicker fiber.[34,43] If the feed rate alone is increased too high, Taylor cone and fiber formation are not stable. The jet needs a longer time to dry from the solvent, and the fibers on the collector can be fused together resulting in a web. When using a lower feed rate the jet has more time to evaporate the solvent and the resulting fibers will be thinner.[49] During the process, the voltage and the feed rate should be at right levels to maintain a stable Taylor cone.[43]

Temperature

The temperature of the solution has a dual impact on to the electrospinning process (Table 2). Higher temperature accelerates the evaporation of the solvent and the result is thereby thicker fibers. At the same time the higher temperature reduces the viscosity which leads to more uniform fibers.[44]

Needle

In the simple electrospinning setup, there is only one needle or spinneret (Figure 4). The inner diameter of the needle has a minor but existent effect on the electrospinning process (Table 2). When choosing a smaller needle to the electrospinning system, also the droplet at the tip of the needle comes smaller. A smaller droplet has a higher surface tension, and a greater part of the voltage goes to the initiation of the jet rather than electrospinning or accelerating the jet. Therefore the fiber has more time for stretching and elongation, and the fibers will be thinner.[42] If the needle diameter is too small, the solution cannot come through it and no fibers are obtained.

In more complex electrospinning setups, there can be multiple spinnerets. These can be made for example by using several needles or spinnerets together[50,51] (Figure 6), or by using a porous hollow tube as a solution container[52,53] (Figure 7). Advantages of this kinds of multiple spinneret setups are the increased productivity and deposition area. Also, multi-component blend nanofiber mats have been made with multi-jet electrospinning.[54] There is also a disadvantage: the jets experience coulombic repulsion with each other and the resulting fiber mat on the collector is not continuous (Figure 6).

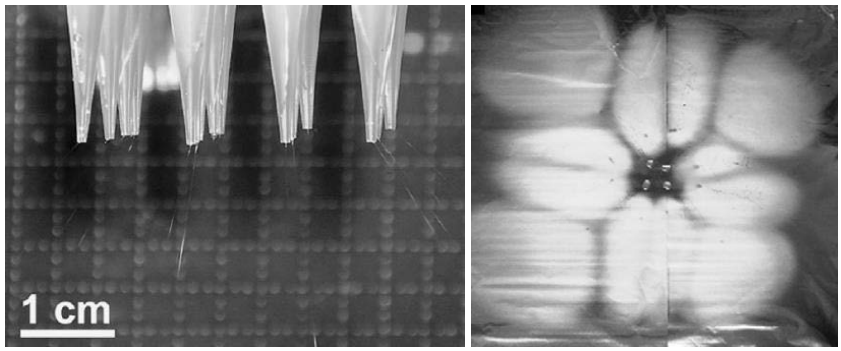

Figure 6 (Left) Image of a multiple spinneret setup. (Right) Multi-jet electrospun fiber mat on the collector. Reprinted from [50] by permission of Elsevier, Copyright (2009).

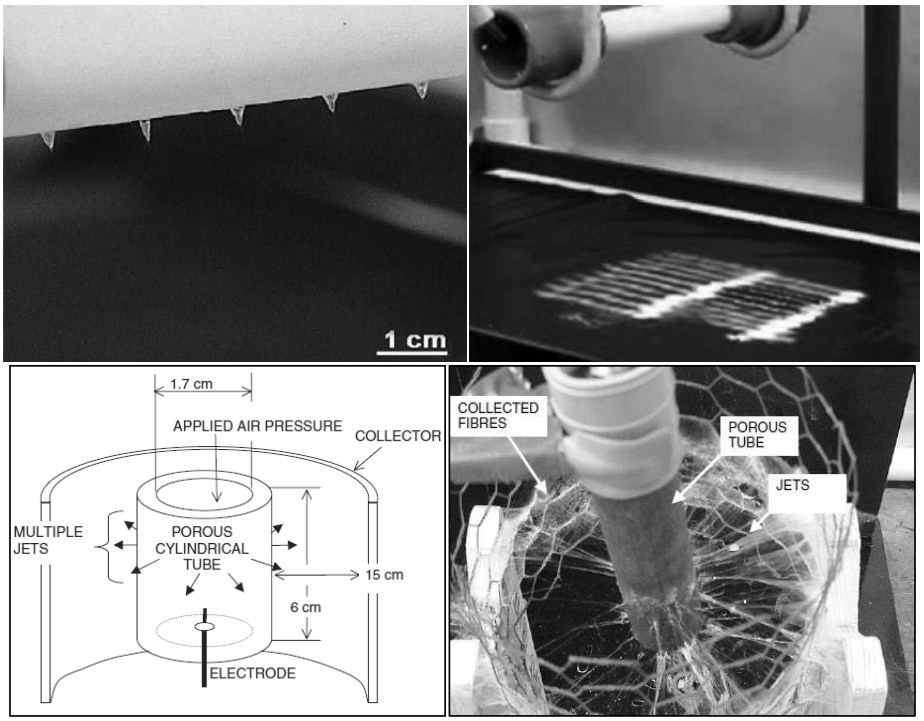

Figure 7 Examples of porous hollow tube electrospinning setups. Upper Figures reprinted from [53] by permission of Elsevier, Copyright (2008). Bottom Figures reprinted from [52] by permission of IOP Publishing, Copyright (2006).

Electrospinning can also be utilized to prepare hollow fibers directly. In this case a spinneret which is consists of two coaxial capillaries is used (Figure 8A).[16] The outer capillary is for the sheath material and the inner capillary for the core material. In a typical procedure, two viscous but immiscible liquids, for example heavy mineral oil in the inner capillary and PVP / $Ti(O^iPr)_4$ ethanol solution in the outer capillary are simultaneously electrospun from the needle to form a coaxial fiber.[16] Hollow fibers are obtained by calcining the composite nanotubes in air (Figure 8).

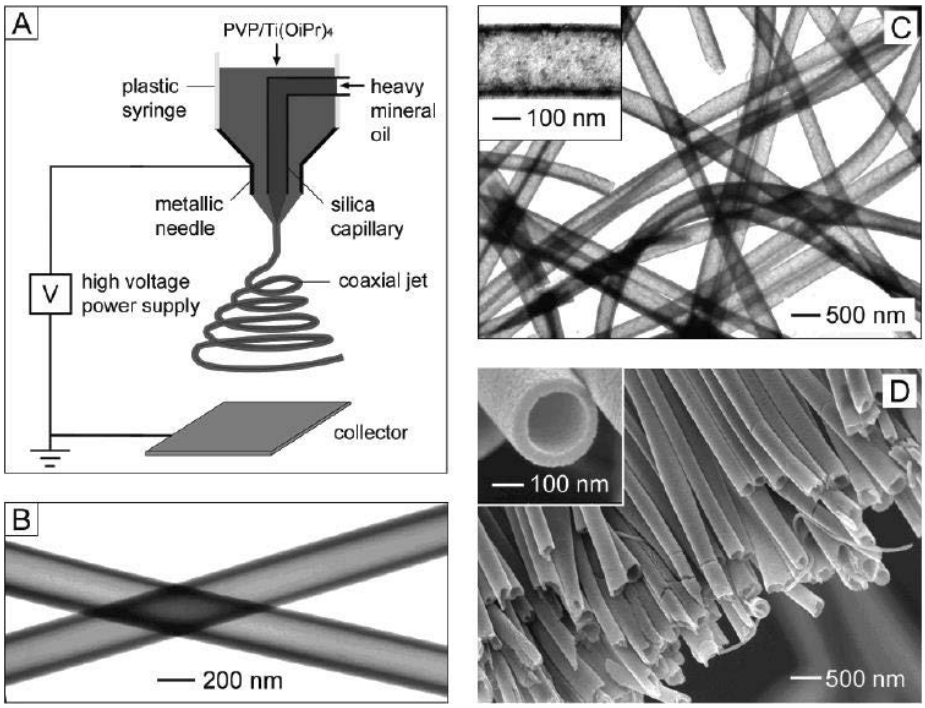

Figure 8 (A) Schematic illustration of the electrospinning setup for direct fabrication of hollow fibers. (B and C) TEM images and (D) SEM image of the fabricated hollow TiO_2 fibers after calcination at 500 °C. Reprinted from [16] by permission of American Chemical Society, Copyright (2004).

Collector

The collector is the third part of the electrospinning system (Table 2). In a simple electrospinning setup, the collector can be some conductive material such as an aluminum foil that is electrically grounded. When the collector is electrically conductive, it is discharging during the process and fibers are collected in high packing density. In turn, if the collector is non-conductive or non-grounded, the collector is charging. Repulsive forces between the fibers causes repulsion of fibers from the surface. As a result, less fibers are deposited on the collector. For the same reason a non-conductive collector causes also a lower packing density of fibers compared to those collected on a conductive surface where charges are dissipated.[45] In some cases, a non-conductive collector and the accumulation of charges causes a formation of three dimensional fiber structures.[55] This can also happen with a conductive collector after it has been coated with a thick layer of non-conductive polymer fibers.

Shape of the collector has also an impact on the resulting fiber-mat. For example, a cylinder collector results in a tube with a wall made of fibers (Figure 9). Structure of the collector is also affecting the result, for example a porous metal mesh as a collector results in a fiber-mat with a low packing density of fibers. This is because the fibers dry faster, and remaining charges on the fibers reject later depositing fibers.

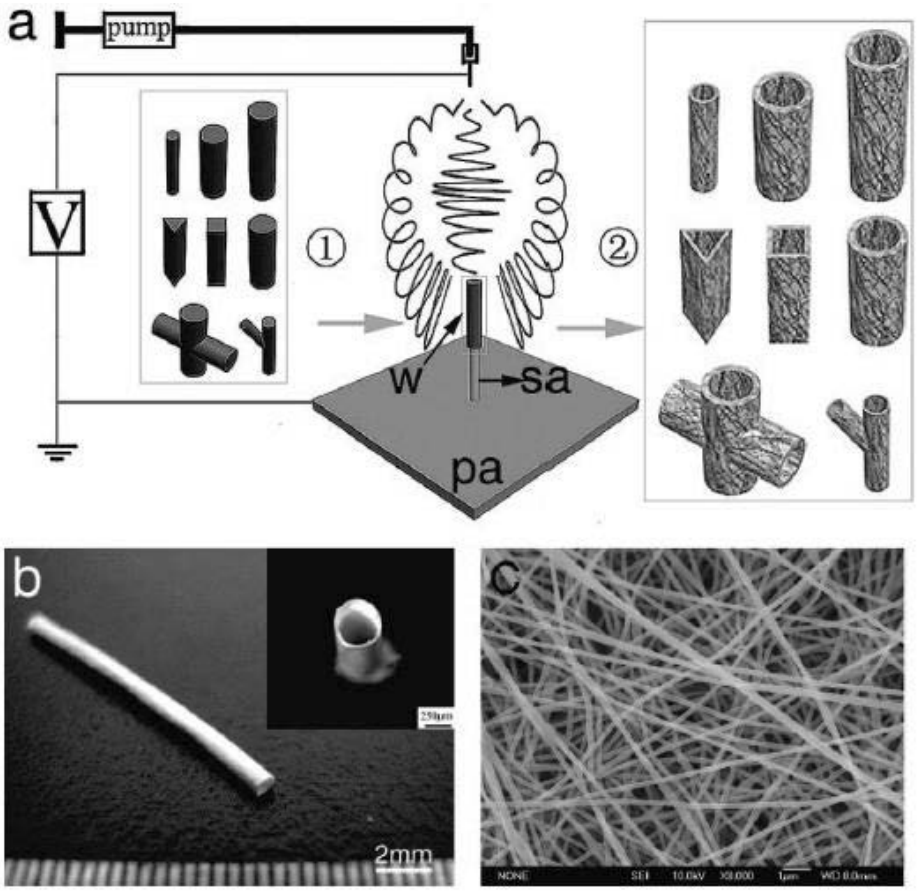

Figure 9 (a) A schematic illustration of fabrication of fibrous tubes by electrospinning using 3D collectors and resulting fibrous tubes. (b) Image of a tube having fibrous walls. (c) SEM image of the tube wall shown in (b). Reprinted from [46] by permission of American Chemical Society, Copyright (2008).

The collector can also have patterns, for example evaporated metal stripes on a glass substrate, or two parallel silicon electrodes with an air gap in between (Figure 10). Electrospinning on this kind of collectors produces highly oriented fibers.[12]

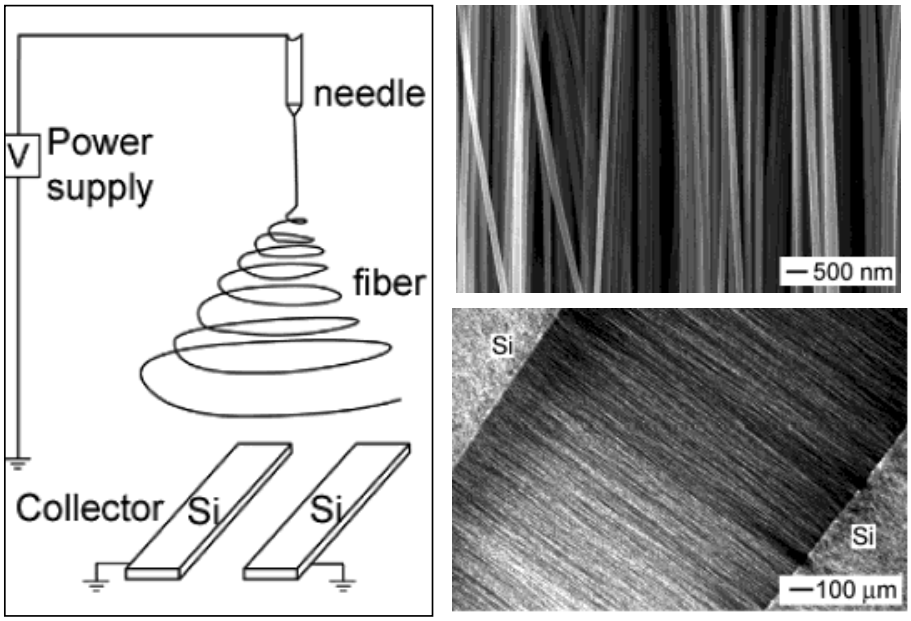

Figure 10 (Left) Schematics of an electrospinning setup with parallel collector electrodes, (Right) SEM-images of electrospun fibers aligned between the collector electrodes. Reprinted from [12] by permission of American Chemical Society, Copyright (2003).

The collector can also be moving instead of being static. The simplest moving type collector is rotating, for example a rotating wire drum (Figures 4C and 11). Fibers collected on a rotating collector are highly aligned (Figure 11).[47] The use of a rotating collector also helps in drying the fibers, because they have longer time to evaporate the solvent before being covered by the next layer of fibers. The rate of evaporation is also increased due to a stream of air that is caused by the rotating motion.[56]

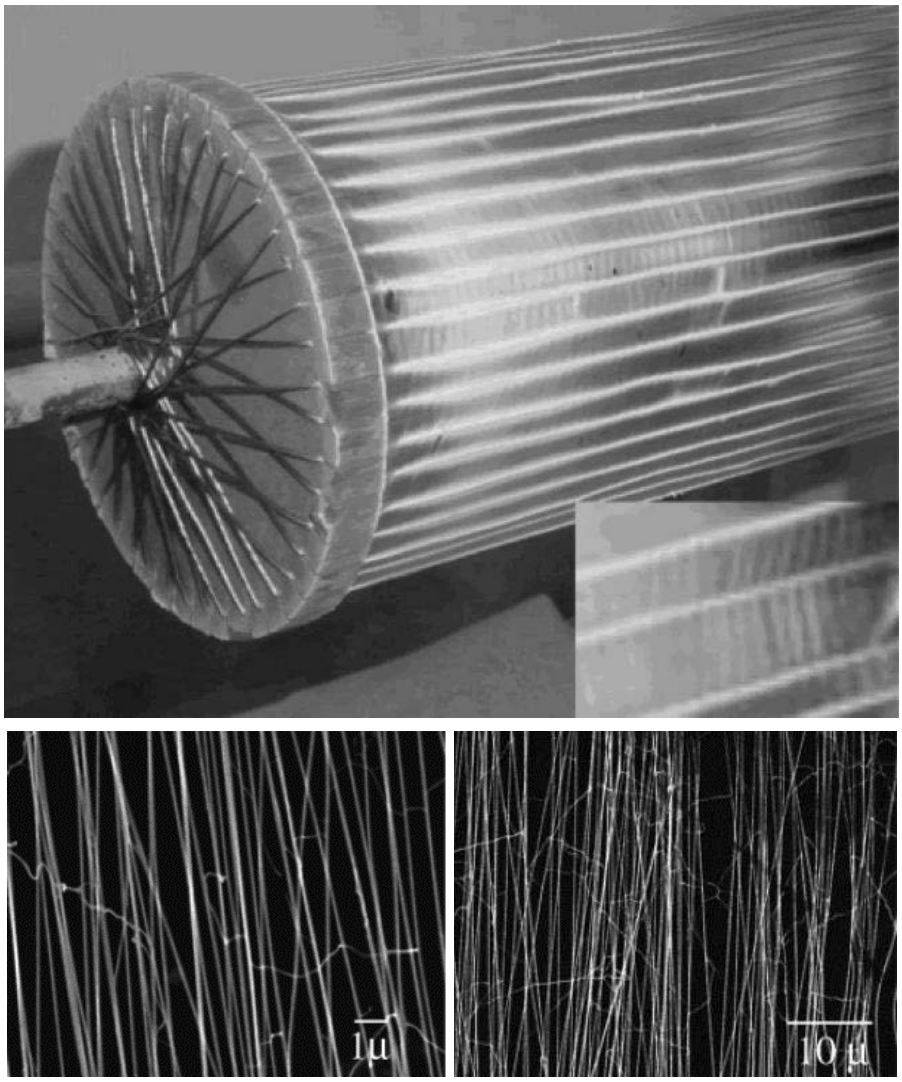

Figure 11 (Top) Image of a rotating wire drum collector and (Bottom) SEM images of aligned electrospun fibers collected with the wire drum. Reprinted from [47] by permission of American Chemical Society, Copyright (2004).

Needle - collector distance

The distance between the needle tip and the collector is the easiest way to adjust the flight time of the electrospun jet (Table 2). When increasing the distance between the needle and the collector, electric field and acceleration of the jet are decreased. Longer needle-collector distance ensures a sufficient flight time for the jet to get well separated fibers. If the flight time is too short, solvent evaporation is incomplete and fibers might fuse together on the collector.[39]

When the distance between the needle and collector is increased, the acceleration of the jet is decreased and the flight time is increased which results in decreased average diameter of the electrospun fibers.[8,42,48] On the other hand making the distance longer can also result in thicker fibers because of too little stretching of the fibers in the low electric field.[40] It is also good to be aware that if the distance between the needle and the collector is too high, charged fibers may end up somewhere else than on the collector.[42]

2.2.3 Ambient parameters

There are also other parameters which may influence the electrospinning process, for example, humidity, ambient atmosphere and pressure. These parameters are still poorly investigated. It has been shown that humidity can cause porosity to the electrospun fibers.[57] A change of the ambient atmosphere may have an influence on the fiber formation, for example electrospinning in a helium atmosphere cannot be successful because the gas starts breaking down electrically already at low voltages. On the other hand, if only the atmosphere is changed from air to a gas which has a higher breakdown voltage, for example Freon®-12 gas, diameters of the fibers are increased, even doubled. The higher breakdown voltage allows the jet to retain its charge for a longer time.[58] Reduced pressure helps flowing the solution and evaporation of the solvent, but it can also be a disadvantage if the droplet gets dried already on the needle tip.[22]

2.3 Materials

The most common material type processed by electrospinning is polymers. Polymers can be easily prepared to a liquid form with a proper viscosity for electrospinning. Other material types made by electrospinning are composites and ceramic materials, and recently also metals. Polymers and most composites are ready to use as such directly after the electrospinning, whereas metals and ceramics require post processes, annealing in particular.

2.3.1 Polymers

Polymers are the most common material type investigated during the history of electrospinning. This is because they are inherently suited to electrospinning, but they are also often inexpensive and commercially available. Polymers can be classified several ways, but here they are divided only into two categories: synthetic polymers and biopolymers.

Synthetic polymers are as the name says synthesized by polymerizing monomers by for example addition polymerization or by condensation polymerization. The most commonly used electrospinning materials are (not in any order) polyvinyl pyrrolidone (PVP), polyvinyl acetate (PVAc), polyvinyl

alcohol (PVA), polyethylene oxide (PEO) and polyamides, for example polyurea (PU) (Figure 12).[11,59]

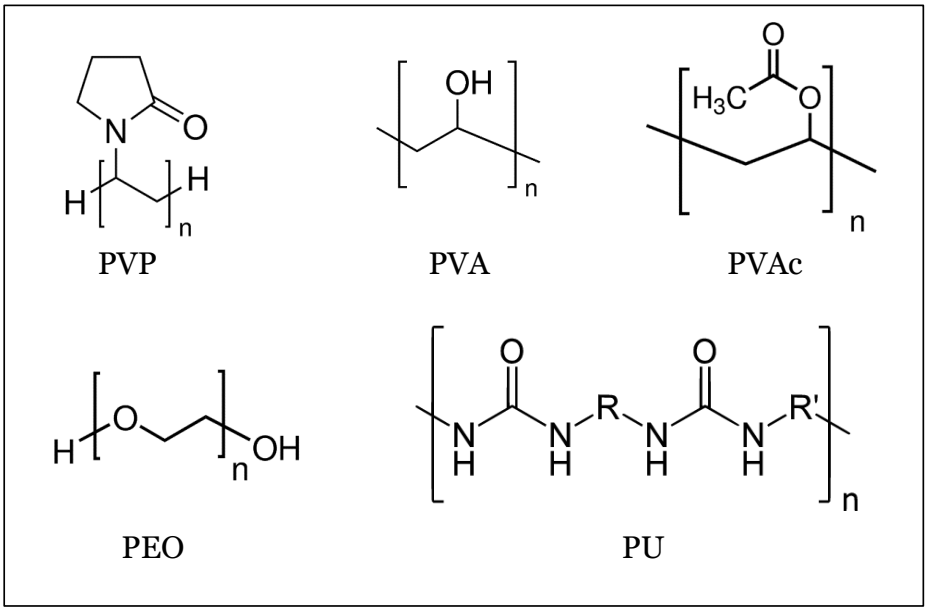

Figure 12 Molecule structures of typical electrospun polymers.

Biopolymers or natural polymers are a rapidly growing topic in the electrospinning research. They have many medical applications, including surface modification of implants, tissue engineering, wound healing, and drug delivery.[10] Some biopolymers, for example collagen, can also be used by blending them to polyethylene oxide (PEO). In addition to collagen, other widely examined biopolymers are for example chitosan, silk and cellulose.[11]

2.3.2 Composites

In the composite materials two or more distinct materials are combined to gain new physical or chemical material properties that the materials cannot provides as individual components. The constituents of the composites remain separate phases without dissolving to each other or forming solid solutions. The main parts of a composite material are called as a matrix and reinforcement. The matrix is a binding material and it gives the shape to the material. The matrix is also acting as a supporting material for the reinforcement components. The reinforcement components are fibers or particles that are mixed within the matrix to give a new property to the composite, for example mechanical, electrical or magnetic properties. Typical example of a composite material is fiber reinforcement of a matrix material, like carbon or glass fiber reinforced polymers and ceramics.[59]

Composite materials can be prepared by several methods including electrospinning. For example, by adding magnetic nanoparticles to the electrospinning solution a normally non-magnetic polymer fiber becomes magnetic,[60] or by adding metal particles to a polymer matrix it is changed to a conductive polymer composite.[61] Electrospun composites may also be called as nanocomposite materials, because the fibers and reinforcement components are typically in the nanometer scale.

2.3.3 Ceramic materials

Electrospinning of ceramic materials has been studied widely. Ceramic materials (oxides,[24] nitrides[62-65] and carbides[66-68]) are non-metallic inorganic materials, for example silicon oxide and biocompatible hydroxyapatite,[69-71] which are composed of metals and non-metal elements like oxygen, nitrogen or carbon. Ceramic materials have many interesting properties which also make them interesting materials to prepare in fiber form by electrospinning. Several ceramics have catalytic properties, for example TiO_2,[72] or they are magnetic materials like $CoFe_2O_4$,[73,II] and some of them are ideal for use as sensor materials, like ZnO.[74] Most of the ceramics are dielectric materials and thus ideal for use as an electrical insulator like alumina, Al_2O_3.[75] There are also some ceramics which are semiconductors and can be used as conductive materials in electronics, for example indium tin oxide, ITO.[76]

Generally, ceramic fibers are electrospun from a polymer solution mixed with a proper amount of metal precursors, for example PVP/ethanol solution and titanium isopropoxide. After electrospinning, fibers are calcined for example in air atmosphere. During the calcination the polymer is combusted, and the metal precursors are oxidized to metal oxides, like TiO_2. The crystallinity of the final product is depending on calcination temperature and time.[77]

Electrospinning directly from sol-gels is an interesting but little studied alternative to the polymer containing precursor solutions for electrospinning of ceramic fibers. Choi et al. described how silica fibers can be electrospun directly from a sol-gel without using any additive polymers.[78] Sol-gel is a chemical process where precursors, typically metal alkoxides and metal salts, undergo various forms of hydrolysis and polycondensation reactions. These reactions lead finally to a solid phase whose morphology ranges from discrete particles in the solvent (a sol) to a continuous inorganic polymer network with solvent trapped inside (a gel). During these reactions, the sol becomes more viscous. At a right moment, when the sol is converting to a gel, the colloid solution has a proper viscosity for electrospinning of ceramic fibers (Figure 13). Though only sparsely used in electrospinning, sol-gel is otherwise widely

used in making thin films and other products from oxides. Therefore, a vast sol-gel recipe literature is available for electrospinning experiments.

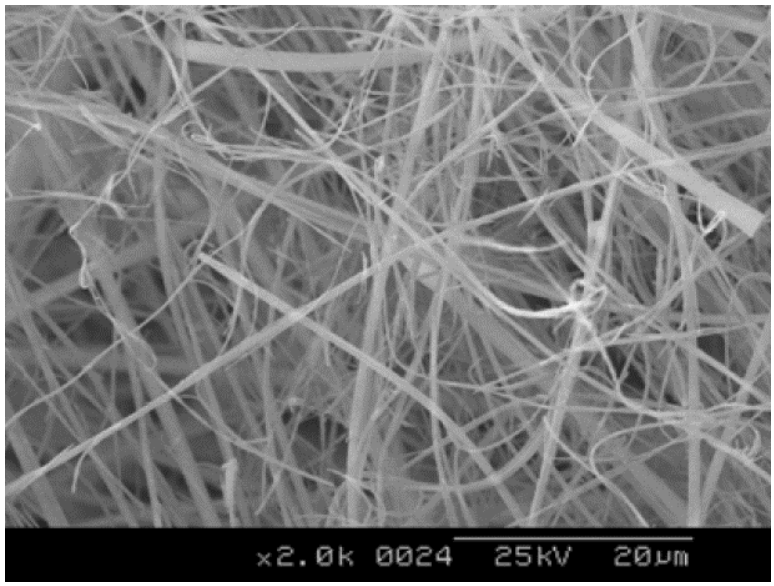

Figure 13 SEM image of silica fibers that were electrospun from a sol. Reprinted from [78] by permission of Springer Nature, Copyright (2003).

2.3.4 Metals

While electrospinning of polymers and ceramics has been widely studied, electrospinning of metals is still poorly explored area. Perhaps the most important property of metal nanowires is their good electrical conductivity, and therefore they can be used as conductors in many electrical applications. There are only a few papers that are reporting electrospinning processes for metals, most of them being noble metals (Ir, Pt, PrRh, PtRu and Au),[III,79-83] but also metallic Cu fibers have been prepared.[84]

Similar to ceramic fibers, also metals are electrospun from a polymer solution mixed with one[III,79,80,82-84] or several[80,81] metal precursors. For example Shui et al.[79] and Kim et al.[80] prepared Pt fibers by electrospinning PVP-ethanol solution which contained H_2PtCl_6. In most cases metal fibers were obtained by calcination in air and consecutive reduction for example with H_2 gas,[III,79-81,84] but there are also studies where metal fibers were obtained already by direct calcination.[80,81]

2.4 Mass production and scaling up

Electrospinning is a simple method to produce fibers of several materials. However, the basic setup shown in Figure 4A is rather slow for producing large quantities of fibers for industrial purposes. This slowness can be circumvented by using different setups for example by combining together the previously described multiple spinnerets[50,51] (Chapter 2.2.2. – Needle properties) and moving collectors (Chapter 2.2.2 – Collector).[54] Figures 14 and 15 shows different electrospinning setups for mass production. With a proper setup it is possible to produce self-supporting electrospun nonwovens with aa aerial mass in the range of 10 – 250 g/m^2.[85]

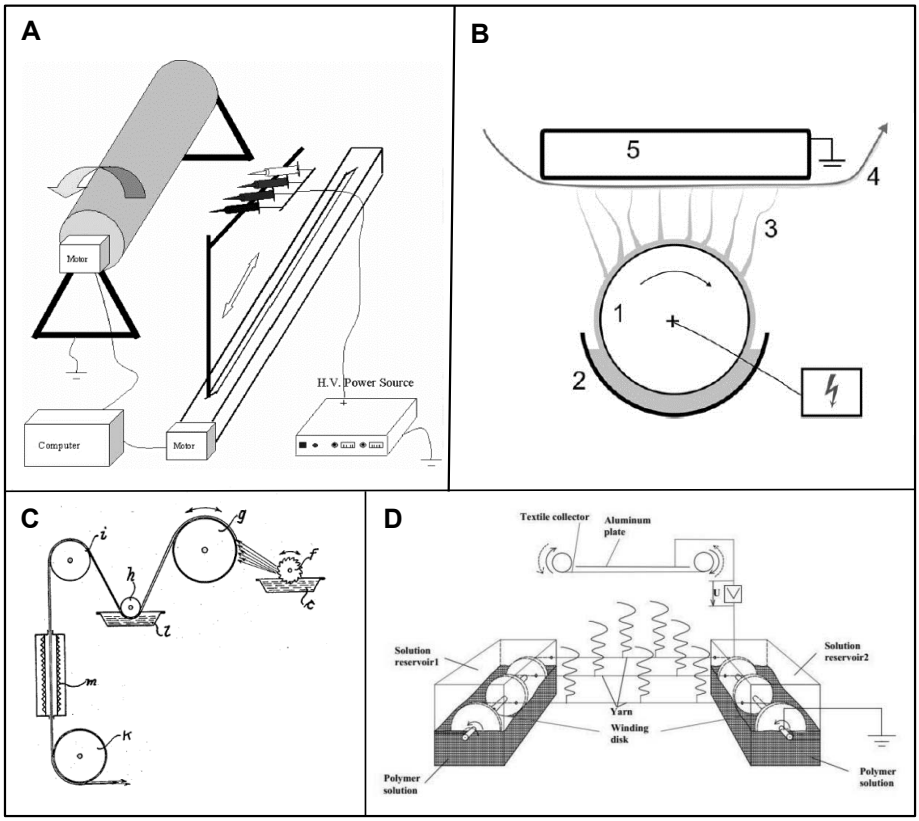

Figure 14 Electrospinning setups where A) both multiple needles and collector are moving, B) charged metal roller acts as a spinneret and a roll to roll web as a collector, C) the spinneret is a serrated wheel and fiber bundles or yarns are collected onto a roll. D) Setup of an electrospinning device with conventional moving yarns as the spinneret. Figure A reprinted from [54] by permission of Elsevier, Copyright (2004). Figure B reprinted from [86] by permission of Elsevier, Copyright (2009). Figure C reprinted from patent [6]. Figure D reprinted from [87] by permission of Springer Nature, Copyright (2018).

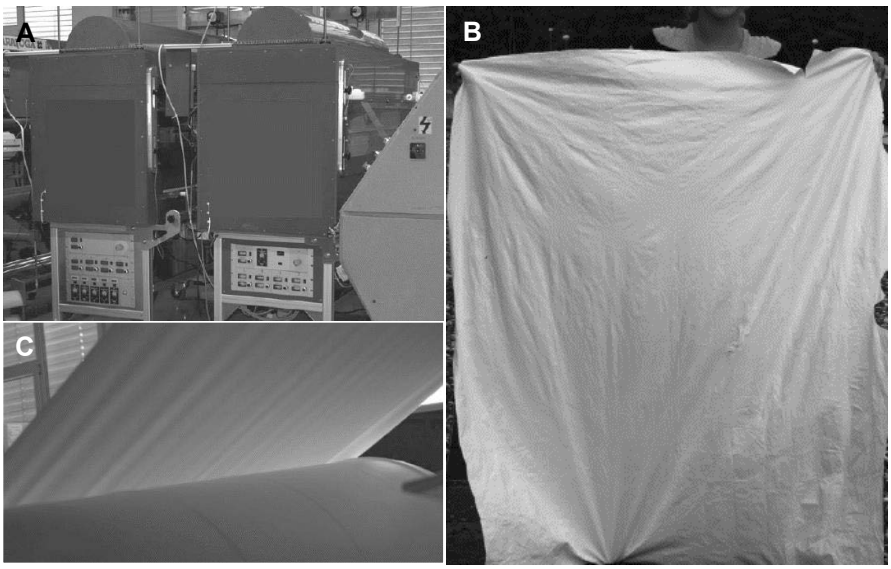

Figure 15 A) and B) Electrospinning device where the collecting fabric can be more than 100 cm wide. C) Image of self-supported PVA nonwoven fiber mat with about 25 g/m^2. Figures A and C reprinted from [88] by permission of John Wiley and Sons, Copyright (2008). Figure B reprinted from [85] by permission of John Wiley and Sons, Copyright (2009).

Many commercial devices, like Elmarco's needle-free Nanospider™ devices are nowadays based on needleless electrospinning.[89] In the needleless electrospinning, the needle is replaced with different types of electrodes, for example a wire electrode in the Nanospider™ device or a twisted wire spinneret in our own setup (Figure 3).[IV] The Nanospider™ device is capable of producing polymer fibers with a rate of about 68 g/h (~600 kg/year) and our own setup theoretically about 5 g/h (43 kg/year).

One of the most interesting modifications of the basic electrospinning process is electroblowing (EB), which is also called as gas-assisted, gas jet or blowing assisted electrospinning.[90-92] In the EB system the normal electrospinning process is assisted with a high velocity gas flow (Figure 16). The solution is pulled with air flow through the needle, fiber formation occurs as a combined effect of electrical field and high velocity gas, and fibers are collected on the wire mesh collector.[90] The solution flow rate in this system is about 30 ml/h which represents over 30-fold increase compared to the conventional electrospinning.[93] When a typical production rate with the normal single needle electrospinning setup is about 0,1 g/h, with a single needle EB the production rate is about 3 g/h. The 30-fold production rate improvement compared to the simple electrospinning makes the EB method very useful in research and development purposes.

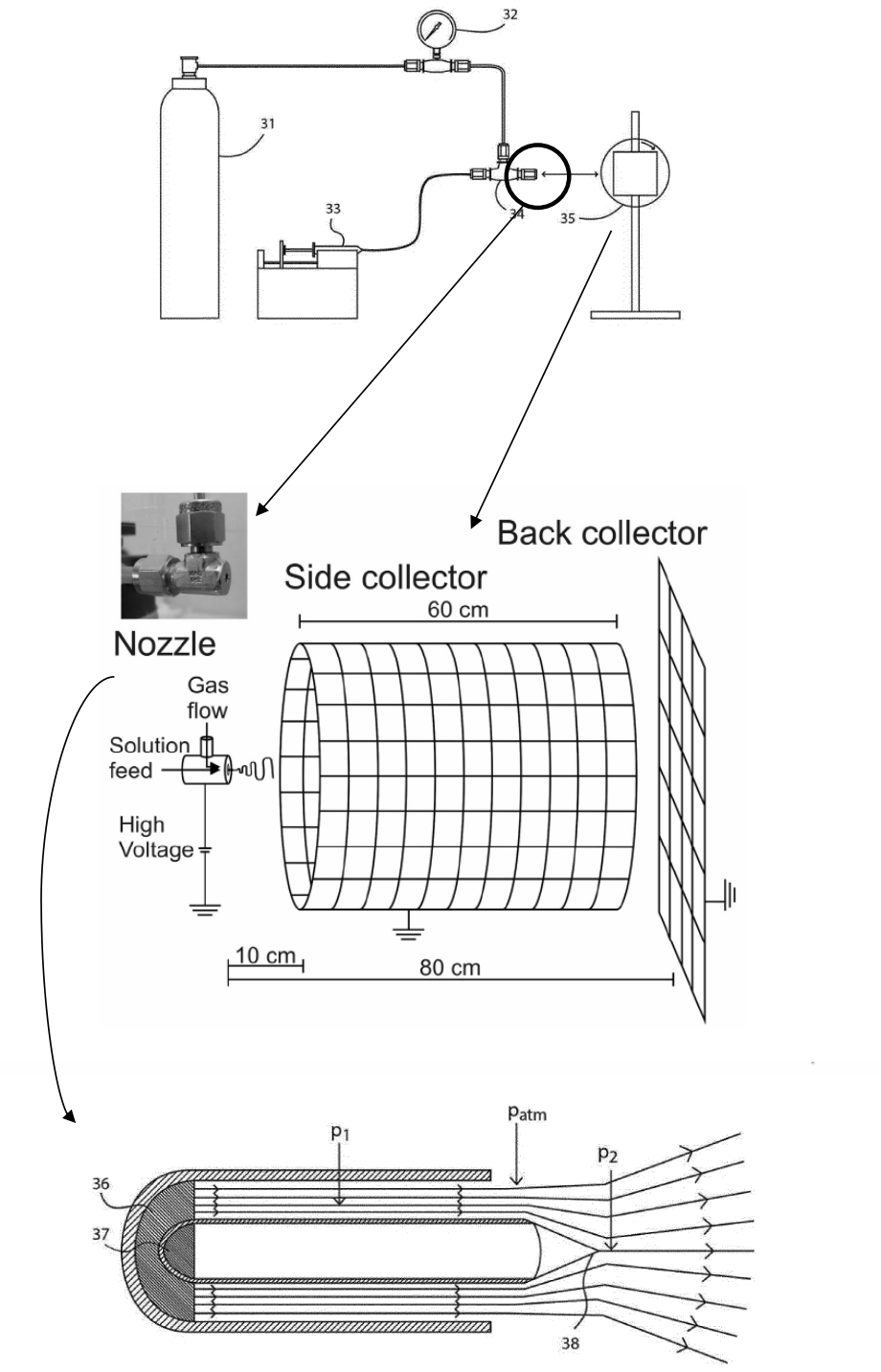

Figure 16 Schematics of electroblowing system.[93-95]

3 ATOMIC LAYER DEPOSITION

Atomic Layer Deposition (ALD)[96-101] is a straightforward method to deposit conformal thin films with atomic layer accuracy. ALD is a method capable to produce numerous thin films types, like metal oxides, nitrides, fluorides, chalcogenides and metals like silver or gold (Figure 17). In industry ALD has many applications in microelectronics, but it is also used in making e.g. electroluminescent (EL) displays and solar cells. ALD is extensively exploited also in nanotechnology. While ALD does not produce nanostructures by itself, the excellent conformality of the method allows coating various nanostructures, including electrospun nanofibers.[I, III]

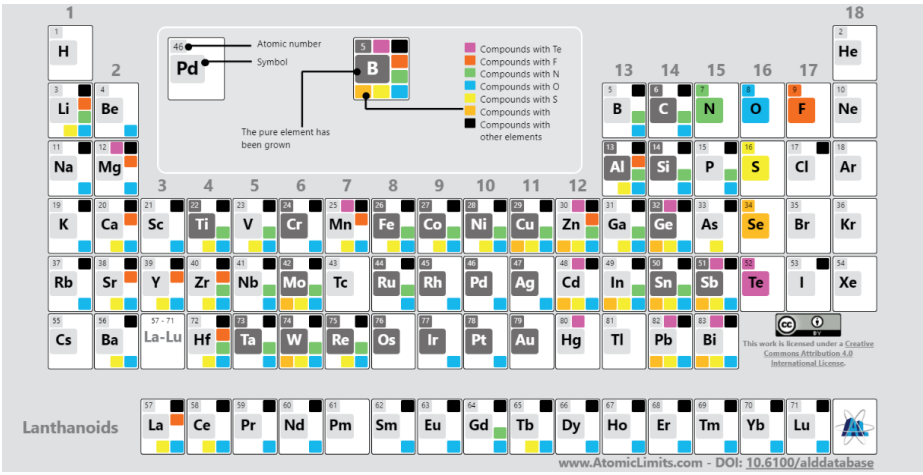

Figure 17 Periodic table of ALD elements and compounds. Reprinted from [102] published under the Creative Commons License BY 4.0.

Characteristic to ALD is that precursor vapors are brought onto the substrate surface alternately, one at a time. Each precursor reacts on the surface in a saturative manner, which makes the film growth self-limiting, that is, the surface chemistry determines how much film material is being deposited in each step. Thanks to the self-limiting growth mechanism, the ALD method fills all requirements that the modern thin film industry needs: **thickness control**, **uniformity**, **conformality** and relatively **low process temperature** (Figure 18).[100] Thickness control is important because film thicknesses in certain applications e.g. in microprocessors have to be atomic layer accurate. Uniformity is needed because substrates are coming larger and larger and thin films must be uniform over the whole substrates. Conformality of thin films means that the thin film thickness should be uniform over trenches and even more complex features like pores

and surface roughness. Low temperatures, for example lower than 100 °C are often also needed, because the substrates e.g. polymer fibers or previously deposited thin films can be damaged at higher deposition temperatures.

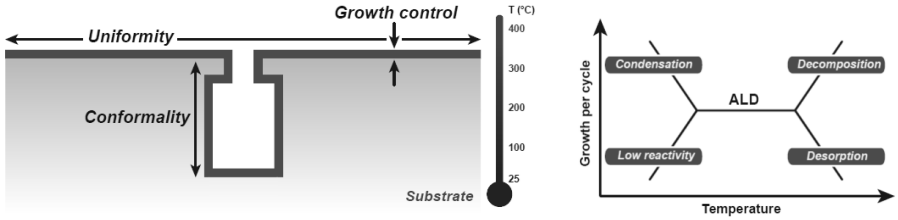

Figure 18 (Left) Schematic picture for growth control in terms of four metrics. (Right) Picture of ALD window. Reprinted from [100] by permission of Elsevier, Copyright (2015).

3.1 ALD process and self-limiting growth

In the ALD process precursors are delivered sequentially onto the substrate surface one by one. Figure 19 shows a schematic picture of one ALD cycle. The precursor in the first half-cycle, for example trimethyl aluminum (TMA), is delivered on the substrate. The precursor reacts with the surface until all possible reaction sites are used and the surface is saturated. Next the excess precursor is purged away. After purging, the other precursor in the second half-cycle, for example water, is delivered on the substrate and reacts with the surface that was formed by the first precursor. Again, excess precursor is purged away, and one atomic layer of the desired material is deposited on the substrate. In reality, however, the thickness of the material deposited in one ALD cycle is often only a fraction of a full monolayer. Anyhow the thickness of thin film is controlled simply and accurately by the number of ALD cycles.

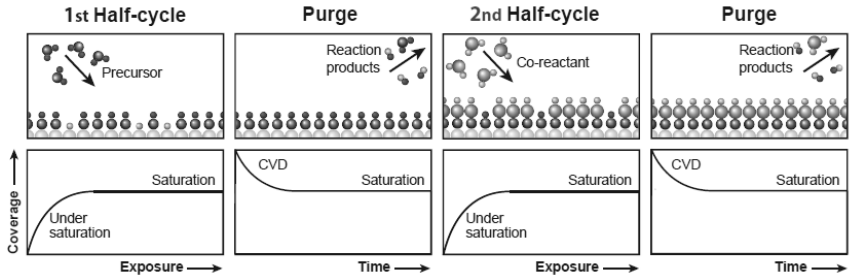

Figure 19 Schematic picture of an ALD cycle (above) and how saturation is achieved with function of time (bottom). Reprinted from [100] by permission of Elsevier, Copyright 2015).

Figure 19 shows also how the requirements of ALD must be fulfilled in each step. The exposure times of the precursors have to be long enough. If the exposure time is too short, the substrate surface is not saturated with the precursor and the film will not be uniform. Also, if purging times are too short, excess precursors on the substrate or in the reaction chamber cause CVD component to the growth and this often also makes the film non-uniform. The sequence times in each step must therefore be long enough to reach saturation and thus the self-limiting growth.[100]

3.2 ALD window

The process temperature is an important factor in an ALD process.[100,101] Figure 18 shows three temperature zones in the growth rate graph: a low temperature zone, an ALD window, and a high temperature zone.

In the low temperature zone, the process temperature is low, and the saturation is not reached because the growth is limited by low reactivity. The low temperature can also cause multilayer adsorption or condensation of the precursor on the substrate. This causes CVD growth which can be seen as a faster growth rate. In both cases the growth rate is strongly depending on the process temperature.

The middle temperature zone is called as an ALD window. In this zone the saturation is reached, and the growth rate is self-limited over the whole temperature zone. The growth rate of the process can be independent of temperature which is seen as a constant growth rate in the ALD window. However, the growth rate of some processes can also be temperature-dependent, which can be seen as a slight increase or decrease in the growth rate. Temperature range of the ALD window is important to know when selecting the substrate material for a given process, for example in the case of electrospun polymer fibers.

In the high temperature zone, the growth rate is again strongly depending on the process temperature. High temperatures can cause precursor decomposition and CVD reactions on the surface. Alternatively, high temperatures can cause precursor desorption and thereby a decrease of the growth rate.

4 EXPERIMENTAL

4.1 Electrospinning apparatus

Electrospinning was done by a self-made apparatus that consists of a high voltage power supply (Gamma High Voltage Research Inc. ES30P - 5W/DDPM, voltage range from 0 to +30 kV), a metal grid or silicon wafer as a sample collector, a plastic syringe, a 22 gauge metal needle, and a syringe pump (KD Scientific KDS-230) (Figure 20).

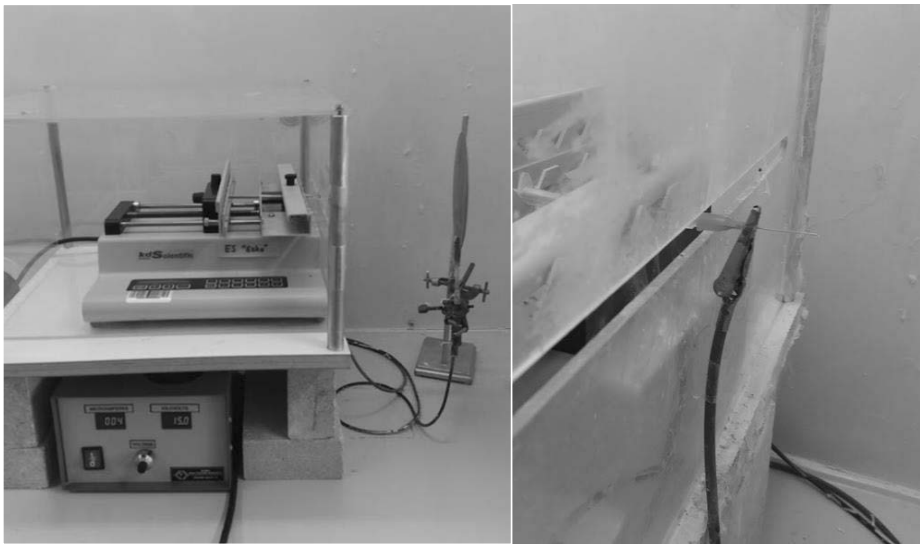

Figure 20 Electrospinning set-up. 1. high voltage power supply, 2. syringe pump, 3 syringe and needle, 4. high voltage connector, and 5. grounded collector.

4.2 Electrospinning of fibers

Electrospinning process was done by placing the electrospinning solution, for example polymer solution with selected metal precursors, into the plastic syringe. The solution was then delivered to the metal needle at a constant flow rate by using the syringe pump. The needle – collector distance was set to 10 - 15 cm and the needle was connected to the high voltage (10 – 15 kV). Fibers were collected onto silicon wafers. When an inorganic final product was aimed for, the fibers were calcined in air at 500-600 ° C for 4 hours.

Table 3 shows the inorganic materials that we have electrospun successfully. We have also electrospun some bare synthetic and natural polymers (Table 4). In the case of bare polymer fibers, there is no need of calcination; the electrospun fibers are ready right after the electrospinning process.

Table 3. *Electrospun inorganic fiber materials made in this work.*

Electrospun material	Precursor/Solvent / Polymer	Distance (cm)	Voltage (kV)	Ref.
TiO_2	$Ti(O^iPr)_4$ / EtOH / PVP	15	12	14
$BaTiO_3$	$Ti(O^iPr)_4$ + $Ba(ac)_2$ / EtOH / PVP	15	15	103,104
SnO_2	$SnCl_4 \cdot 5H_2O$ / H_2O / PVA	10	10	105
CuO	$Cu(NO_3)_2 \cdot 3(H_2O)$ / H_2O+^{i}PrOH / PVB	20	25	84
IrO_2	$Ir(acac)_3$ / Acetone + EtOH / PVP	15	15	III
ZnO	$Zn(ac)_2 \cdot 2H_2O$ / H_2O+EtOH / PVP	20	20	106
Fe_2O_3	$Fe(acac)_2$ / Acetone + EtOH / PVP	10	15	II
$NiFe_2O_4$	$Ni(acac)_2$ + $Fe(acac)_2$ / Acetone + EtOH / PVP	10	15	II
$CoFe_2O_4$	$Co(acac)_2$ + $Fe(acac)_2$ / Acetone + EtOH / PVP	10	15	II
SiO_2	TEOS / EtOH + HCl / no polymer	10	10 - 16	78
Al_2O_3	$Al(acac)_3$ / Acetone + EtOH / PVP	10	15	107

Table 4. *Synthetic and natural polymers that have been electrospun in this work.*

Polymer	M_w (g/mol)	w-%	Solvent	Distance (cm)	Voltage (kV)	Ref
PVP	1300000	7	EtOH	15	15	14, I - III
PVA	80000	10	H_2O	15	15	108
PVAc	500000	14	DMF	15	15	109
PEO	300000	5	H_2O	15	15	30
PMMA	350000	10	Acetone	15	15	110
PMMA	350000	10	$CHCl_3$	15	15	111
PVB	80700	7	8:2 ^{i}PrOH : H_2O	20	25	84
Chitosan	250000	8	7:3 TFA : DCM	15	15	112

4.3 ALD coatings

The ALD method was used to prepare inorganic nanotubes and composite nanofibers. Polymeric or composite fibers acted as substrates or templates and were coated with a conformal thin film of the desired inorganic material.

ALD coatings were done with two different ALD reactors. For the TUFT processed nanotubes[I] and composite magnetic photocatalyst fibers[II] the ALD depositions were done with a SUNALE R-150 ALD reactor (Picosun Ltd, Finland). Ir/IrO_2 and Pt/PtO_x ALD coatings in paper III were made with a hot wall flow-type F-120 ALD reactor[96,97] (ASM Microchemistry, Ltd., Finland). In both reactors nitrogen was used as a carrier and purging gas.

Table 5 shows the deposited materials, the substrate fibers and the reactors as well as process parameters. Inorganic nanotubes were achieved by removing the template fibers by calcination after the ALD deposition. This was done typically at 500 °C in air for four hours.

Table 5. *ALD coatings deposited on electrospun fibers in this work.*

Material	Substrate	Reactor	Pulsing sequence	Pulse times (s)	Temperature (°C)	Ref.
Al_2O_3	PVP	R-150	TMA – N_2 – H_2O – N_2	0.1 – 2 – 0.1 – 4	150	I, 113
TiO_2	PVP + $CoFe_2O_4$	R-150	$TiCl_4$ – N_2 – H_2O – N_2	0.2 – 10 – 0.2 – 10	250	II, 114
Ir	PVP	F-120	$Ir(acac)_3$ – N_2 – O_2 – N_2	2 – 1 – 2 – 1	225	III, 115
Ir	Al_2O_3/PVP	F-120	$Ir(acac)_3$ – N_2 – O_2 – N_2	2 – 1 – 2 –1	225	III, 115
IrO_2	PVP	F-120	$Ir(acac)_3$ – N_2 –O_3 –N_2	2 – 2 – 2 – 2	165	III, 116
Ir	PVP	F-120	$Ir(acac)_3$ – N_2 –O_3 –N_2 –H_2 – N_2	2 – 2 – 2 – 2 – 6 – 2	165	III, 117
PtO_x	PVP	F-120	$Pt(acac)_2$ – N_2 – O_3 – N_2	4 – 4 – 2 – 4	120	III, 118

4.4 Characterization

The morphology and structure of the synthesized products were examined by field-emission scanning electron microscopy / scanning transmission electron microscopy (FESEM / STEM, Hitachi S4800), transmission electron microscopy (TEM, FEI Tecnai F30 ST at 300 kV), and X-ray diffraction (XRD,

PANalytical X'Pert PRO, equipped with a Cu Kα source (λ = 1.5405 Å)). Film thickness (in paper I) was measured with XRR (Bruker D8 Advanced X-ray diffractometer). Quick monitoring of the fiber formation and alignment was done with an optical microscope (Olympus BX51). Thermogravimetric analyses were done with a Mettler Toledo Star System with a TGA 850 Thermobalance. Further details can be found from the corresponding papers.

Photocatalytic activities were tested by decomposing methylene blue (MB) in aqueous solution. Decomposition was done by using a UV lamp with radiation wavelengths 340–410 nm (a peak maximum at 365 nm). The distance between the UV source and the sample cuvette was set to one centimeter. The decomposition of MB was followed during the UV-radiation by an UV–vis-spectrophotometer. For the spectrophotometer measurements the solution and fibers were separated by a strong permanent magnet (Figure 21).

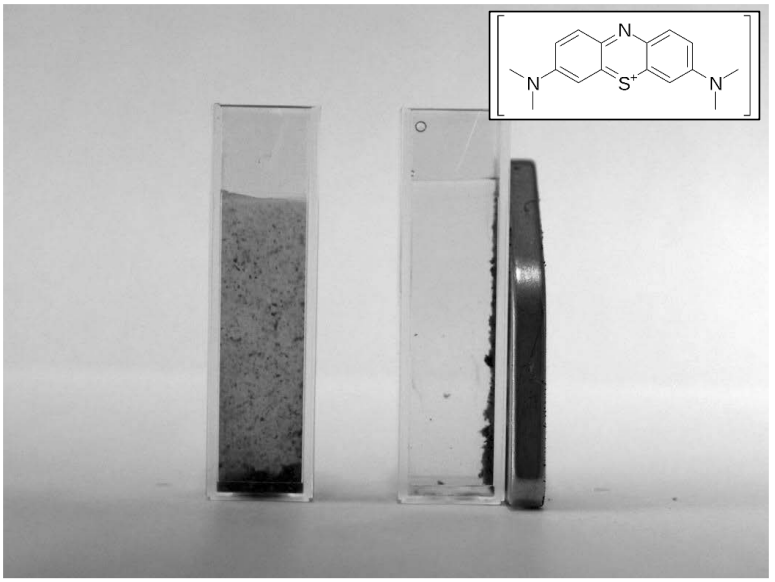

Figure 21 Image showing how a strong magnet separates the fibers from the solution. Inset presents the molecule structure of methylene blue, MB. Reprinted from [II] by permission of IOP Publishing, Copyright (2009).

5 RESULTS

This chapter summarizes the main results of the thesis. More details about the experimental work and the results can be found from the corresponding papers (I-V).

5.1 Electrospinning of nanofibers

The aim of the first part of this study was to construct the electrospinning setup (Figure 20) and verify its operation by electrospinning different materials. Various recipes from literature were tested and own recipes were developed too, Table 3 and Table 4.

5.1.1 Constructing and testing of the electrospinning setup

The basic setup of the self-made electrospinning apparatus has been described in Chapter 4.1. It consisted of a plastic syringe with a metal needle, a syringe pump to control the flow rate of the precursor solution, a high voltage power supply, and a simple fixed collector, for example a silicon wafer.

The operation of the setup was verified by electrospinning PVP/ethanol solution that contained acetic acid and titanium(IV)isopropoxide.[14] The needle-collector distance was 10 cm and the processing voltage was 10 kV. The electrospun fibers were calcined in air at 500°C for 4 hours. FESEM image in Figure 22 verifies the successful operation of the setup.

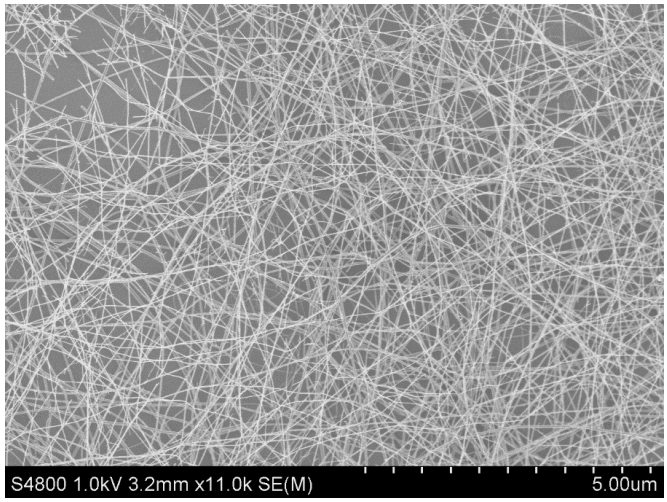

Figure 22 FESEM image of electrospun TiO_2 fibers after calcination.

When other electrospinning process parameters, applied voltage and needle – collector distance were tested, the fiber formation followed the same trends as presented in Table 2 (Chapter 2.2.2). An increase of the applied voltage produced thinner fibers, and also when the distance between the needle and the collector was increased the fiber diameter decreased (Table 6 and Figure 23).

Table 6. *Effect of applied voltage and needle – collector distance on the diameter of fibers.*

#	Applied voltage / kV	Needle - collector distance / cm	Variation of fiber diameter / nm	Average diameter / nm
E1	**9**	10	100 - 300	150
E2	**10**	10	50 - 200	100
E3	**18**	10	40 - 500	100
E4	**24**	10	20 - 50	50
E2	10	**10**	50 - 200	100
E6	10	**15**	40 - 150	100
E8	10	**20**	30 - 100	100

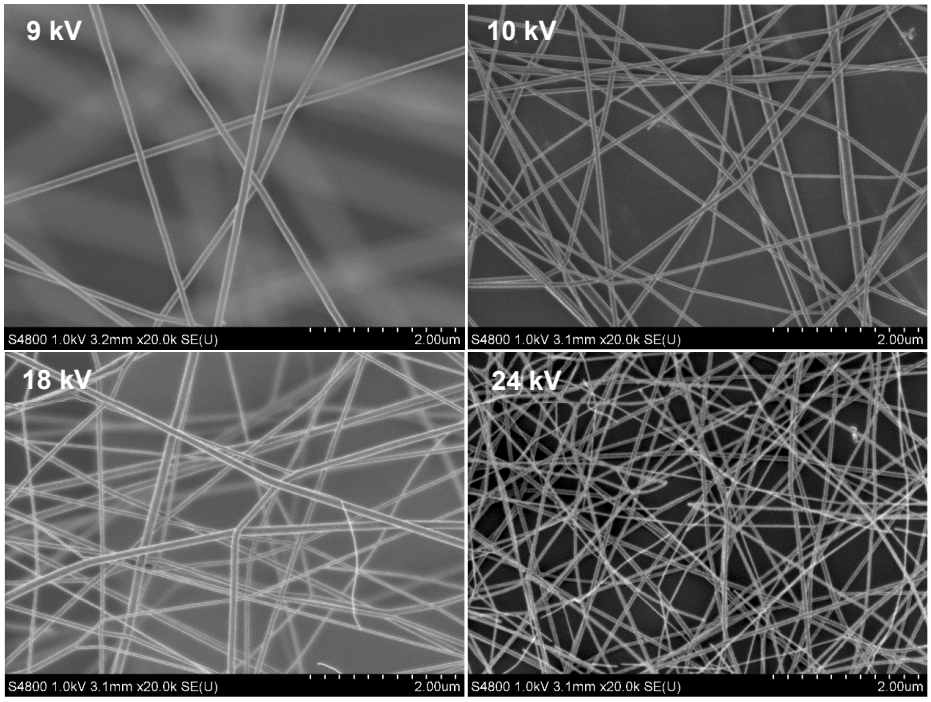

Figure 23 FESEM images of electrospun and calcined TiO_2 fibers when the applied voltage was 9, 10, 18 and 24 kV.

5.1.2 Rotating collectors

After constructing and verifying the operation of the basic setup, it was modified by several different rotating collectors and substrate holders for collection of larger amounts of fibers. The rotation of the collectors was implemented by using an electric motor from a screw twister. The rotation speed could be adjusted continuously from 0 rpm to about 200 rpm.

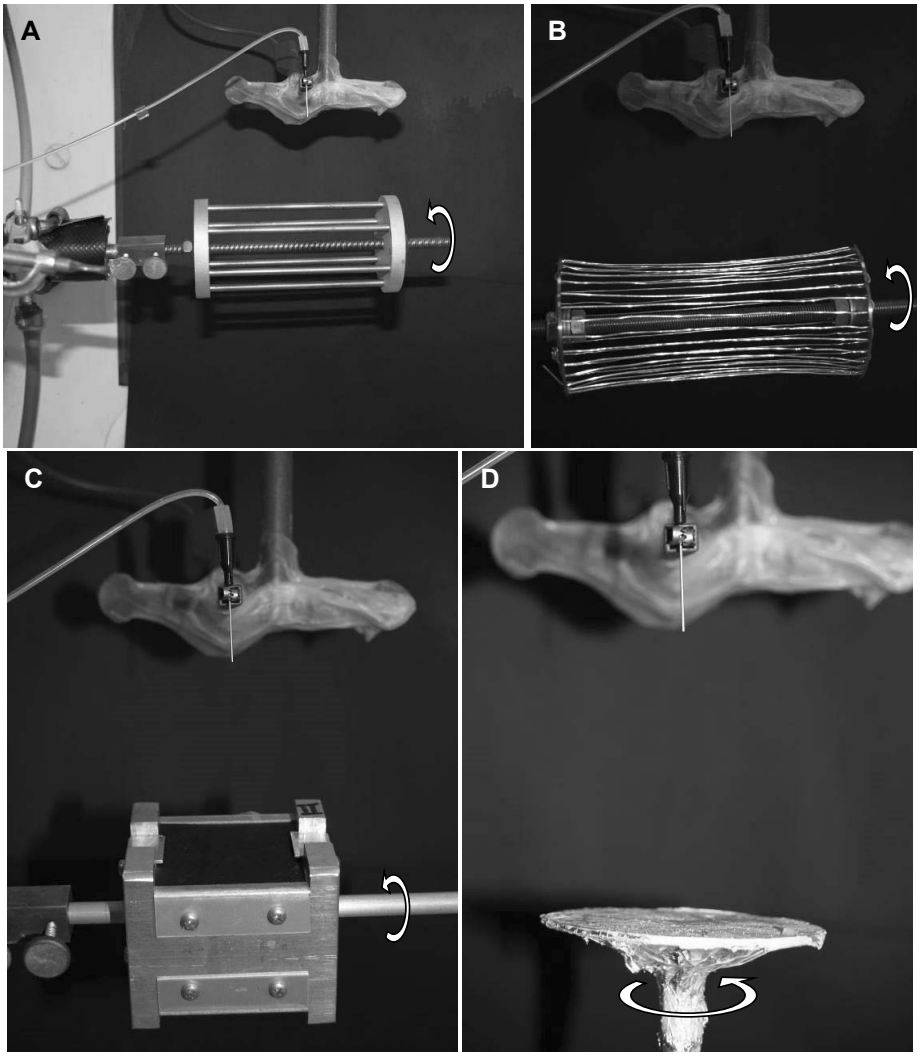

Figure 24 Photographs of different rotating collectors. Arrows indicate the rotating directions.

Figure 24 shows different rotating collectors. In Figure 49A there is a wire drum which is made from thick (5 mm) metal wires with 25 mm gaps in between the wires. The use of this wire drum was problematic because fibers

were collected frequently only on the separate wires but not between them. The next development step was a wire drum having smaller gaps between the wires (Figure 24B). This wire drum was made from thin (1 mm) metal wires with 6 mm gaps. Diameters of the both drums were 60 mm and their lengths were 110 mm and 140 mm. The use of the final wire drum in Figure 24B was successful: the fibers were electrospun nicely between the wires and the drum could collect large quantities of fibers. Figure 24C shows a rotating sample holder developed for flat substrates (50 mm x 50 mm) like silicon and glass. It holds two substrates at the same time. Figure 24D shows an image of a rotating flat collector that can be wrapped with an aluminum foil, or another substrate can be attached to it by an adhesive tape.

5.1.3 Fiber alignment

In certain applications it is important to be able to align the fibers. For example, in gas sensors fibers must be aligned between electrodes.[119]

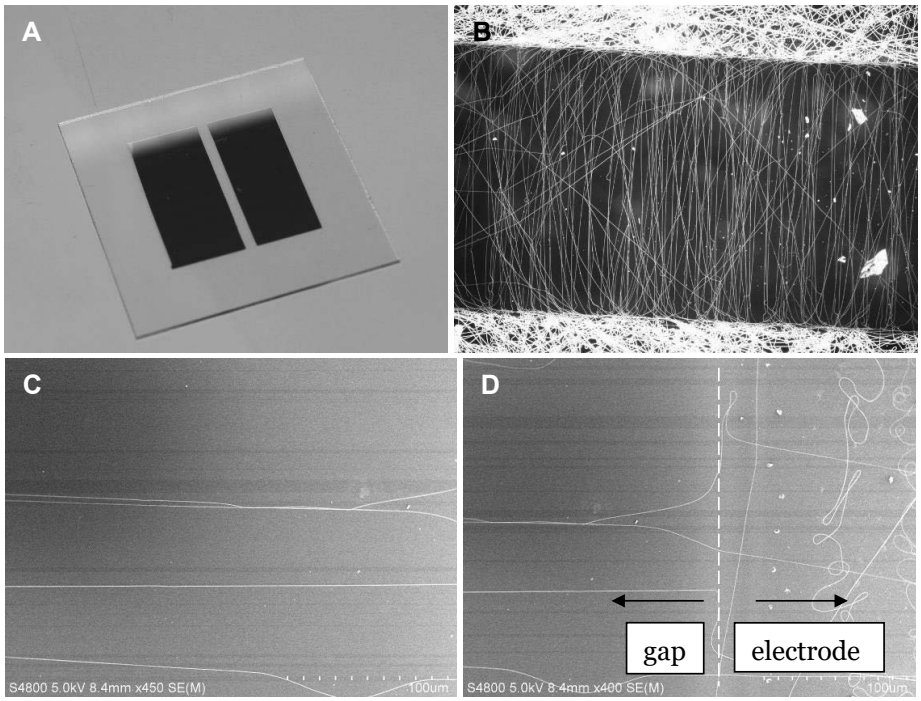

Figure 25 (A) Photograph of the electrode structure for aligning tests. (B) Optical microscope image of aligned fibers between two aluminum electrodes. The gap between the electrodes is 2 mm. (C) FESEM image of aligned fibers within the gap. (D) FESEM image of fibers at the gap - electrode interface.

In this study, alignment of fibers was tried in several ways. The first attempt exploited two grounded metallic electrodes on a glass substrate (Figure 25A). The aluminum thin film electrodes were prepared by using a thermal evaporator and a self-made shadow mask. Figures 25B, C and D show that the alignment is at some level successful, but still far away from the high orientation seen e.g. in Figure 10. The aligned fibers, for example those in Figure 25D, were electrospun on the static non-rotating collector, and the electrospinning time was only 10 seconds. With longer electrospinning times it was important that the electrodes on the substrate were also grounded. Figure 26 shows how fibers were collected non-aligned when the electrodes were not grounded.

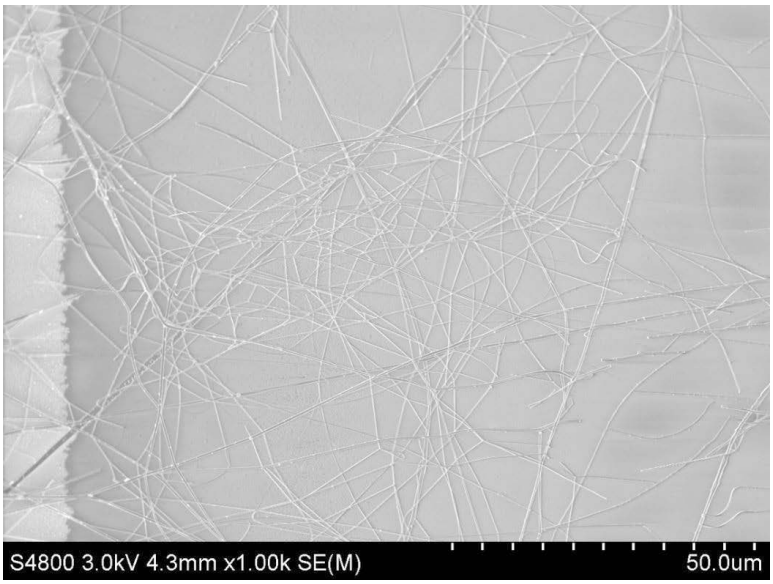

Figure 26 FESEM image of electrospun fibers collected when the electrodes were not grounded. Aluminum electrode is the light area at the left.

Another way to produce aligned fibers is to use a rotating collector. The first attempt with the rotating collector was made using two similar glass substrates with the aluminum electrodes. The substrates were attached to the rotating sample holder shown in Figure 24C, and the electrospinning was done with 10 cm distance and 10 kV voltage. However, it appeared that this kind of a setup did not provide any improvements to the alignment.

The next attempt was made with the rotating wire drum (Figure 24B) as a collector. Fibers were successfully collected on the drum (Figure 27A) when the electrospinning was done with 15 cm distance and 15 kV voltage. When the electrospun fiber mat was thin enough the fibers were aligned (Figure 27B, yellow lines are indicating the fiber direction), but when the electrospun fiber

mat came thicker the aligned fibers became covered with unaligned fibers (Figure 27C). The most likely reason for this behavior is that the electrodes became covered and isolated with the fibers and the later coming fibers could not get in contact with the grounded electrodes anymore.

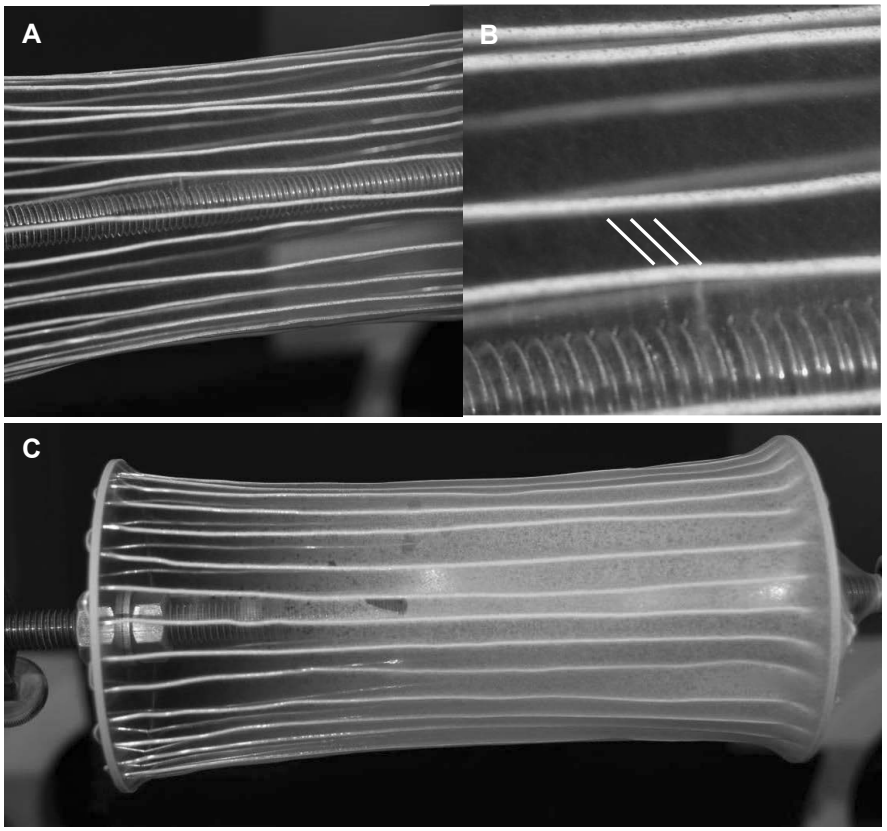

Figure 27 (A) Image of the rotating collector after 5 minutes electrospinning. (B) Magnification reveals aligned fibers. (Yellow lines indicate the direction of the alignment.) (C) The rotating collector after one-hour electrospinning.

Fiber alignment turned out to be quite challenging, and we managed to align fibers only partly. The best way to align electrospun fibers was to use static substrates with conductive and grounded electrodes, as Figure 25 verifies, but even this worked with only a small amount of fibers.

5.2 Needleless twisted wire electrospinning (IV)

The aim of this work was to increase the production rate of the electrospinning process. With the basic single needle setup,[26] the production rate is rather low, only 0.1 – 1.0 g/h. In recent research production rates have been increased by using multiple needles or various needleless systems where, instead of a single jet, multiple jets are simultaneously formed.[51,90,120-128] In principle it is quite straightforward to increase the productivity and deposition area by using multiple needles, but there is a disadvantage: coulombic repulsions between the jets cause noncontinuous fiber mats. Our approach to increase the electrospinning production rate was to use a metallic twisted wire as the spinneret (Needleless Twisted Wire Electrospinning, NTWE, Figure 28).[IV] In general, mass production and scaling up setups have been discussed in Chapter 2.4.

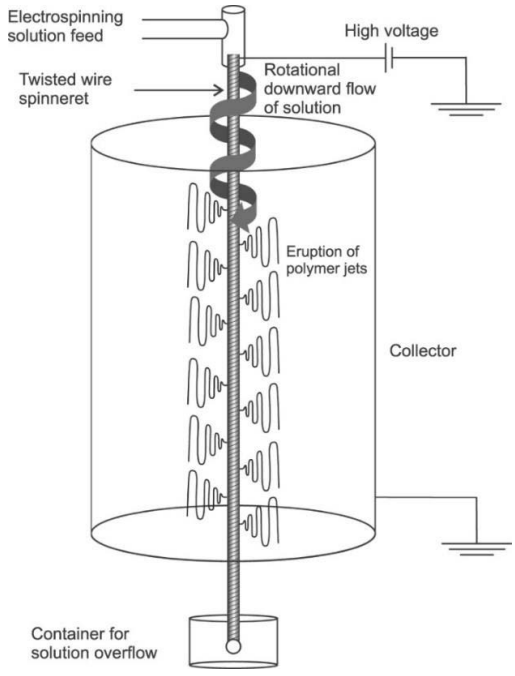

Figure 28 A schematic diagram of a needleless twisted wire electrospinning setup showing the main components of the system. The polymer solution is fed to the top of the twisted wire that acts as the spinneret. Multiple jets are formed and collected on the cylindrical collector around the wire. Reprinted from [IV] by permission of IOP Publishing, Copyright (2015).

Our Needleless Twisted Wire Electrospinning setup consists of a high voltage power supply, syringe pump, twisted metal wire from which multiple polymer jets are erupted, and grounded cylindrical metal grid as the collector (Figures 28 and 29). The electrospinning precursor solution is brought to the top of the vertically aligned twisted spinneret. Due to the gravity, the solution flows downward on the wire and is simultaneously rotating as guided by the twists in the wire. The equipment is simple and straightforward to use. There are no moving parts except the syringe pump and solution itself.

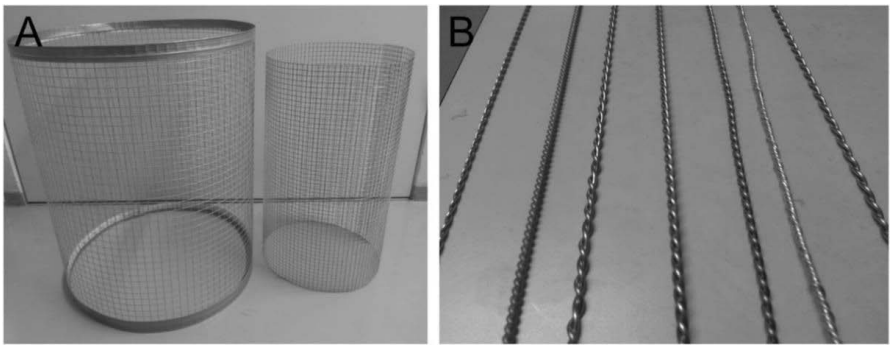

Figure 29 Photographs of cylindrical metal grid collectors and selfmade twisted wire spinnerets. Reprinted from [IV] by permission of IOP Publishing, Copyright (2015).

During the NTWE process, when high voltage is applied to the twisted wire spinneret, jets are ejected simultaneously from multiple Taylor cones self-formed on the downward flowing solution on the wire. Fibers forming from all jets are collected onto the grounded collector that surrounds the spinneret. Because all Taylor cones are moving downwards and rotating as guided by the spinneret, a smooth and continuous fiber mat forms (Figure 30). A video of the process is included to the supporting material of Paper IV.

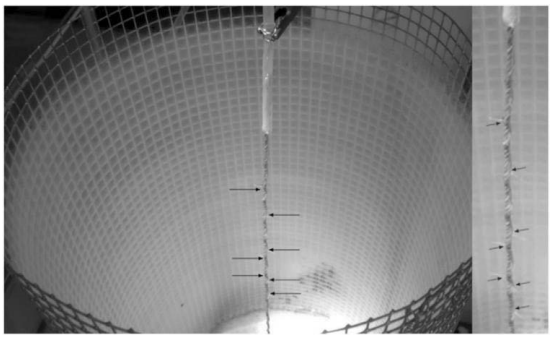

Figure 30 Jet formation from a PVP solution flowing down on the twisted wire during the electrospinning process. Arrows indicate the eruption points observed in the image. The collector is coated with an electrospun fiber mat. Reprinted from [IV] by permission of IOP Publishing, Copyright (2015).

In the simple single needle electrospinning setup, a typical solution feed rate is 0.5 – 2.0 ml/h and with 10 wt% PVP/EtOH the production rate is only 0.14 g/h. With NTWE we tested feed rates from 2 ml/h up to 150 ml/h. The 150 ml/h feed rate was found too high, because the solution was flown over the whole wire and down to the table, and the feed rate was therefore limited to 100 ml/h. The highest production rate 5.23 g/h was obtained by electrospinning 10 wt% PVP/EtOH solution with the 100 ml/h feed rate. The

NTWE method is also useful in production of large area fiber sheets. Depending on the size of the collector cylinder, the area of fiber sheets can be varied largely. In this study the collector gave a fiber sheet with an area of approximately 40 x 120 cm^2 (Figure 31).

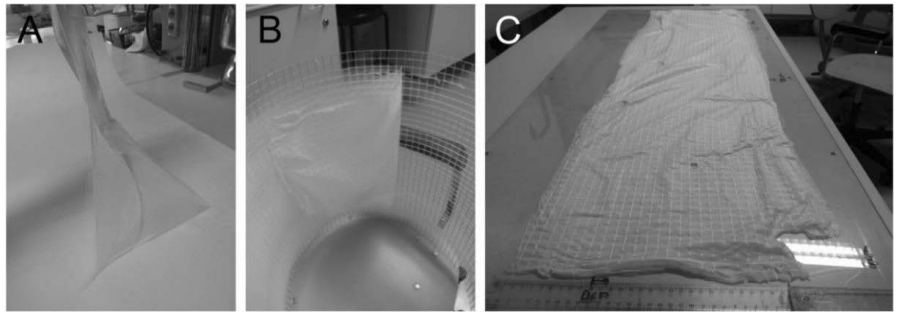

Figure 31 Photographs of (A) a fiber mat being extracted from a surface of a paperboard on which it was electrospun, (B) fibers electrospun directly onto the metal grid collector, and (C) a fiber mat extracted from the collector with an area of approximately 40 × 120 cm^2. Reprinted from [IV] by permission of IOP Publishing, Copyright (2015).

The NTWE process has been tested with both inorganic and polymeric fibers (hydroxyapatite, bioglass and polyvinyl pyrrolidone). These have been electrospun successfully, and the setup can be adapted also to other materials that can be prepared by the conventional electrospinning.

5.3 Nanotubes by combining ALD and electrospinning (I)

The aim of this work was to demonstrate for the very first time the use of electrospun fibers as templates in the ALD process (Figure 2). This is so-called Tubes by Fiber Template (TUFT) process[5,10] which is a very versatile way to produce nanotubes. Earlier the TUFT process had been executed by several methods but not with ALD. The inner diameter of the resulting tube is determined by the polymeric template fiber and the tube wall thickness by the film thickness. For the film deposition ALD offers the highest uniformity and conformality as well as atomic layer accuracy in controlling the film thickness.

A successful TUFT process requires that the template fiber maintains its morphology during the ALD coating. Poly(vinyl pyrrolidone), (Figure 32, PVP, M_w ~ 1 300 000 g/mol) was selected as the template polymer because it is commercially available and well suitable to this kind of process. Its melting temperature is high, around 300 °C, and it has good solubility into water, ethanol and other common solvents. The high melting temperature makes it possible to use PVP in a large number of ALD processes.

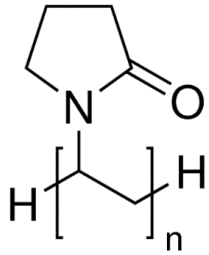

Figure 32 Structure of poly(vinyl pyrrolidone).

In this work Al_2O_3 thin films were deposited on electrospun PVP fibers by the well-known TMA/H_2O ALD process. The fibers were prepared first by electrospinning 7 w-% PVP/ethanol solution, while the needle-collector distance was 10 cm and the voltage 10 kV. After electrospinning, the fibers were coated with Al_2O_3 at 150 °C by using ALD. The ALD-coated fibers were finally calcined in air at 500 °C for 3 h to remove the PVP fiber templates.

FESEM and STEM images (Figure 33) show clearly that the ALD process was successful. Film thickness was measured from the FESEM image and with XRR from a reference silicon sample. These thicknesses were about 100 nm and matched well together. The STEM image proves that the final product is really a tube with a diameter of about 500 nm.

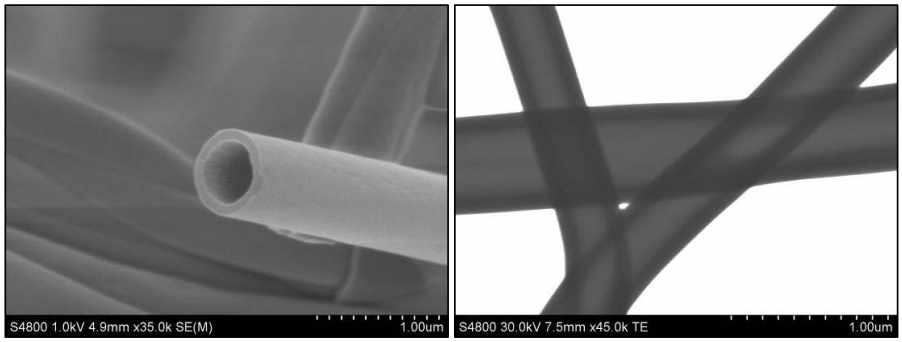

Figure 33 FESEM (left) and STEM (right) images of TUFT processed Al_2O_3 nanotube. Reprinted from [I] by permission of Elsevier, Copyright (2007).

In addition to Al_2O_3, we also prepared TiO_2 nanotubes in a similar manner. TiO_2 thin films were deposited on PVP fibers by the $TiCl_4/H_2O$ ALD process at 250 °C. As before, the ALD-coated fibers were calcined in air at 500 °C for 4 h. The product was TiO_2 tube as the FESEM image in Figure 34 illustrates. The targeted tube wall thickness was 100 nm and as can be seen in the FESEM image the wall thickness is indeed about 100 nm.

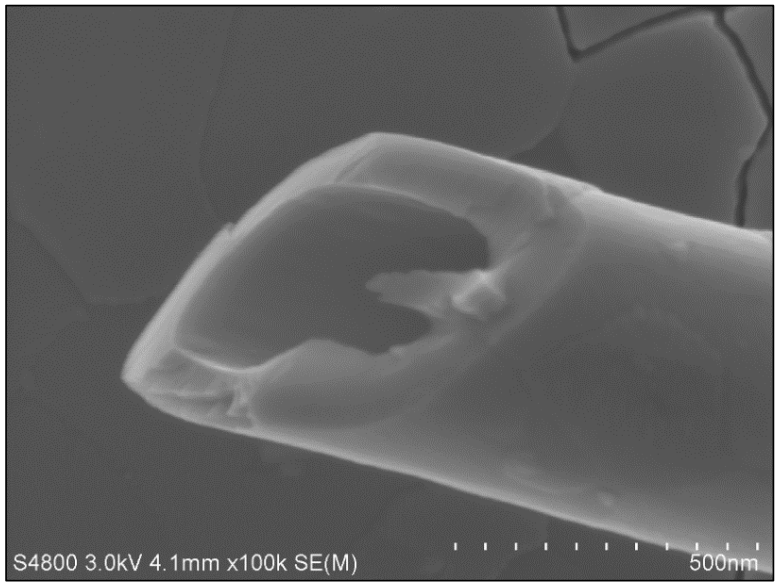

Figure 34 FESEM image of TUFT processed TiO_2 nanotube.

It can be concluded that the TUFT process can be easily done by the electrospinning and ALD methods.[129,I] Subsequently e.g. Peng et al.[113] and Kim et al.[130] have reported on the same procedure and nowadays it is well-known method to prepare tubes.[131]

5.4 Magnetic photocatalyst fibers (II)

The aim of this study was to prepare magnetic photocatalyst composite fibers that can be easily recycled. TiO_2 shell of these fibers acts as a photocatalyst which decomposes pollutants in for example water. Magnetic core is exploited to collect the fibers from water with a magnet for reuse.

TiO_2 thin films were deposited on three kinds of electrospun magnetic core fibers by the $TiCl_4/H_2O$ ALD process. The core fibers were electrospun from a PVP/ethanol solution that contained precursors for the magnetic material. The electrospinning was done with 15 cm needle-collector distance and 15 kV voltage. After the electrospinning the fibers were calcined in air at 500-600 °C for 4 h. After calcination the fibers were coated with TiO_2 by using ALD. The result after the thin film deposition was a coaxial nanowire with the magnetic core fiber and the photocatalytic TiO_2 shell (Figure 35b). Alternatively, the order of ALD and calcination could be changed resulting in only partially filled tubes (Figure 35c).

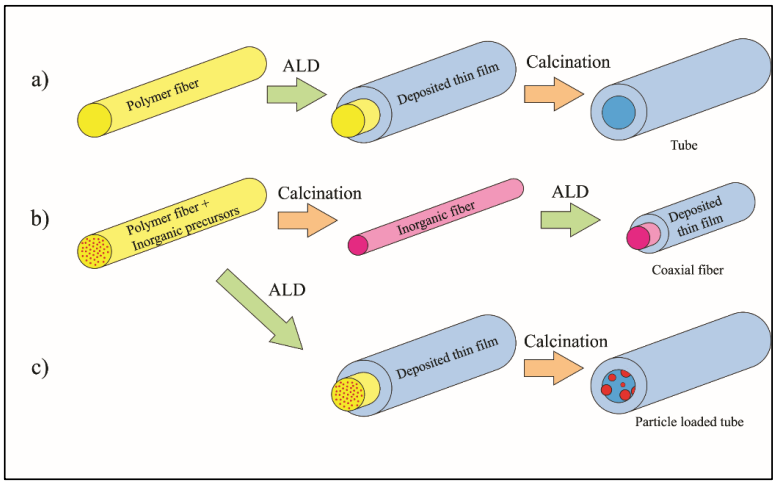

Figure 35 Schematic picture how to combine electrospinning and ALD to prepare different types of nanostructures. Reprinted from [II] by permission of IOP Publishing, Copyright (2009).

5.4.1 TiO_2 coated $NiFe_2O_4$ fibers

Nickel ferrite, $NiFe_2O_4$ is a cubic ferrimagnetic oxide. It is magnetically stronger than for example paramagnetic Fe_2O_3.[13,108] $NiFe_2O_4$ fibers were electrospun successfully from $Ni(acac)_2/Fe(acac)_2$/PVP-solution. FESEM images in Figure 36 show that diameters of the calcined fibers are about 200 nm and their surfaces are smooth. XRD verified that the core material was $NiFe_2O_4$. After the ALD TiO_2 coating it was tested with a strong permanent magnet that the fibers could be collected with a magnetic field.

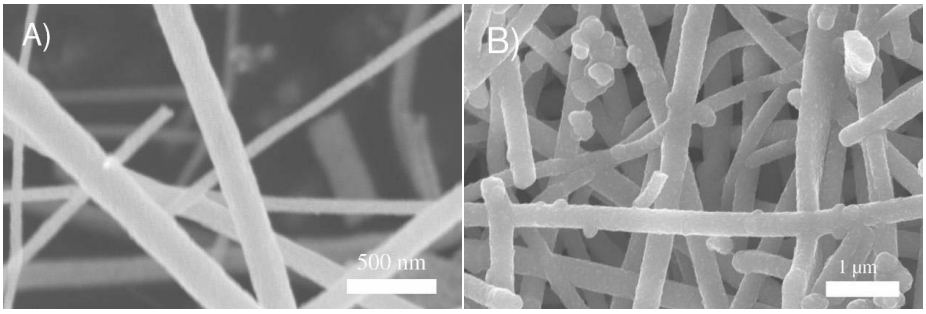

Figure 36 FESEM images of electrospun $NiFe_2O_4$ fibers (A) and TiO_2 coated $NiFe_2O_4$ fibers (B). Reprinted from [II] by permission of IOP Publishing, Copyright (2009).

Photocatalyst tests were done by decomposing methylene blue (MB) in aqueous solution with UV light. However, decomposition of MB with the TiO_2 coated $NiFe_2O_4$ fibers was problematic because the fibers were so heavy that they sank to the bottom of the cuvette. This was avoided by stirring the solution with a magnetic bar, but it seemed that the fibers were somehow broken because the photocatalytic activity could be detected only in the first experiment, but not anymore in reuse after the first collection.

5.4.2 TiO_2 nanotubes filled with $CoFe_2O_4$ nanoparticles

Because of the dispersion problems of the TiO_2 coated $NiFe_2O_4$ fibers, improvement was sought by preparing TiO_2 nanotubes filled only partly with the magnetic core. This was achieved by doing the ALD coating before the polymer was removed by calcination (Figure 35c).

Because the nickel precursor of the $NiFe_2O_4$ fibers was volatile at the ALD process temperatures, this precursor solution could not be used. Instead, $CoFe_2O_4$ was chosen as the magnetic core. Cobalt ferrite is a ferromagnetic material and thus magnetically even better than $NiFe_2O_4$.[13,132] To avoid the sublimation of the cobalt ferrite precursors during the ALD process involatile cobalt and iron nitrates were chosen as precursors.

$CoFe_2O_4$ fibers were electrospun from a PVP/ethanol solution containing stoichiometric amounts of $Co(NO_3)_2{\cdot}6H_2O$ and $Fe(NO_3)_3{\cdot}9H_2O$. Diameters of the calcined fibers, measured from FESEM images (Figure 37), were about 300 nm and surfaces of the fibers were quite smooth. XRD verified that in Figure 37 the fiber material was $CoFe_2O_4$ (Figure 38).

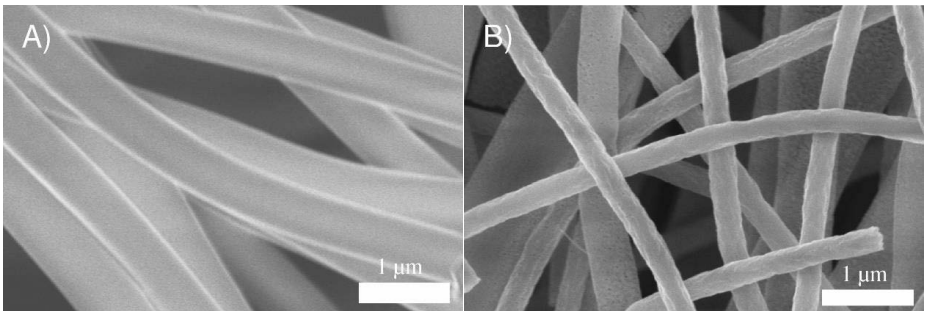

Figure 37 FESEM images of as-electrospun $Co(NO_3)_2/Fe(NO_3)_3$ /PVP composite fibers (A) and $CoFe_2O_4$ fibers after calcination (B). Reprinted from [II] by permission of IOP Publishing, Copyright (2009).

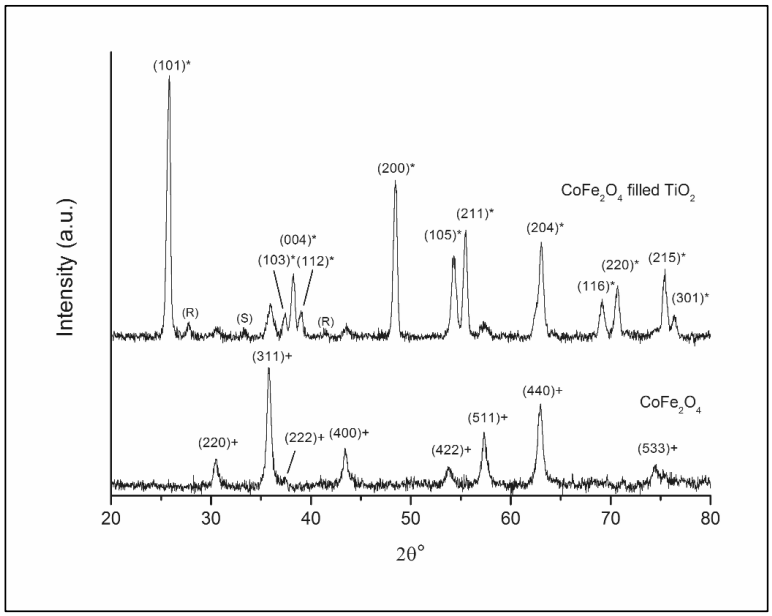

Figure 38 XRD of electrospun $CoFe_2O_4$ fibers and partly $CoFe_2O_4$ filled TiO_2 nanotubes, (∗) anatase TiO_2, (+) cubic $CoFe_2O_4$ (R) rutile TiO_2 and (S) supporting silicon wafer that is used during XRD-measurement. Reprinted from [II] by permission of IOP Publishing, Copyright (2009).

To prepare only partly filled and therefore light enough TiO_2 nanotubes, the fibers were coated with ALD before the calcination. FESEM and STEM images proved that the final product after the calcination was a nanotube loaded with particles (Figure 39). The tube wall thicknesses were about 100 nm and inner diameters about 300 nm. XRD verified the presence of TiO_2 and nanocrystalline $CoFe_2O_4$ (Figure 38) which together with the STEM image (Figure 39) gives a strong prove for the successful preparation of TiO_2 nanotubes loaded with $CoFe_2O_4$ particles. Again, magnetization was verified with a strong permanent magnet.

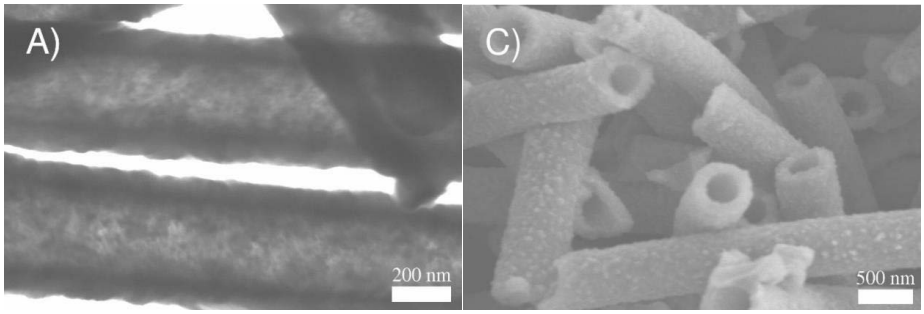

Figure 39 (Left) STEM and (Right) FESEM images of $CoFe_2O_4$ loaded TiO_2 nanotubes. Reprinted from [II] by permission of IOP Publishing, Copyright (2009).

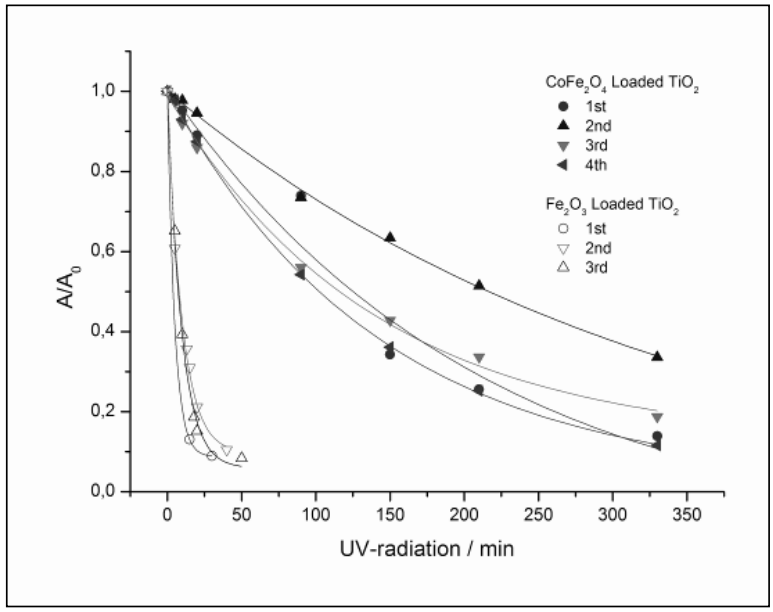

Figure 40 Photocatalytic degradation curves of methylene blue (MB) in repeated experiments after collection of the fibers. Reprinted from [II] by permission of IOP Publishing, Copyright (2009).

Photocatalytic activity of the $CoFe_2O_4$ loaded TiO_2 nanotubes was also tested by decomposing MB with UV-light (Figure 40). After each decomposition test, the fibers were collected with a magnet (Figure 21) and dispersed into a fresh solution of MB. Four successful cycles of decomposition clearly show that we managed to make reusable magnetic photocatalyst fibers.

5.4.3 TiO_2 nanotubes filled with Fe_2O_3 nanoparticles

For comparison, we prepared also Fe_2O_3 nanoparticle loaded TiO_2 nanotubes. Fe_2O_3 is a paramagnetic material and thus magnetically weaker than $NiFe_2O_4$ and $CoFe_2O_4$. Fe_2O_3 particle loaded TiO_2 tubes were prepared by first electrospinning $Fe(ac)_x$ / PVP composite fibers, then coating with ALD-TiO_2, and finally calcining (Figure 41).

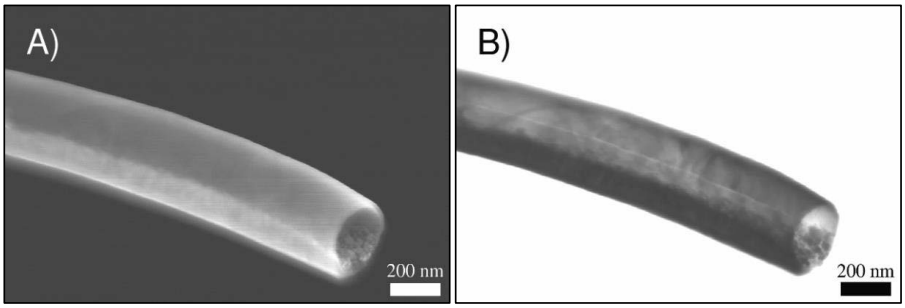

Figure 41 FESEM and STEM images of electrospun and calcined Fe_2O_3 particle loaded TiO_2 nanotube. Reprinted from [II] by permission of IOP Publishing, Copyright (2009).

These Fe_2O_3/TiO_2 tubes showed first much better photocatalytic activity than the $CoFe_2O_4/TiO_2$ nanotubes (Figure 40). However, the synthesis procedure seemed to be quite sensitive, because in the following tests both magnetic and photocatalytic properties were not repeatable. This may be due to a mixing of Fe_2O_3 and TiO_2.

As a summary, composite nanofibers were prepared successfully. The final products acted as photocatalysts and they could be recollected magnetically for reuse. Electrospinning and ALD are a good combination for preparation of this kind of composite materials.

5.5 Ir/IrO_2 and Pt/PtO_x nanotubes and wires (III)

The aim of this work was to show how inorganic and electrically conductive fibers and nanotubes can be prepared simply by using electrospinning only or by using electrospinning - ALD combination in the TUFT process. Noble metals iridium and platinum were selected, because they have both well-known ALD processes and their oxides are also electrically highly conductive.

This study was divided into three parts. In the first part we developed a totally new electrospinning recipe for electrically conductive IrO_2. In the second part we used the TUFT process to prepare Ir and IrO_2 nanotubes by combining the electrospinning and ALD methods. In the last part of this study we prepared also Pt and PtO_x nanotubes by the TUFT process.

5.5.1 IrO_2 and Ir fibers by electrospinning

IrO_2 fibers were successfully electrospun from an $Ir(acac)_3$/PVP solution. The needle-collector distance during the electrospinning was 10 cm and voltage 10 kV. After electrospinning, the fibers were calcined in air at 500 °C for 4 h. The product after the calcination was nanocrystalline IrO_2 nanofiber. Iridium fibers were prepared by exposing the IrO_2 fibers to H_2 gas atmosphere at room temperature for one hour (Figure 42).

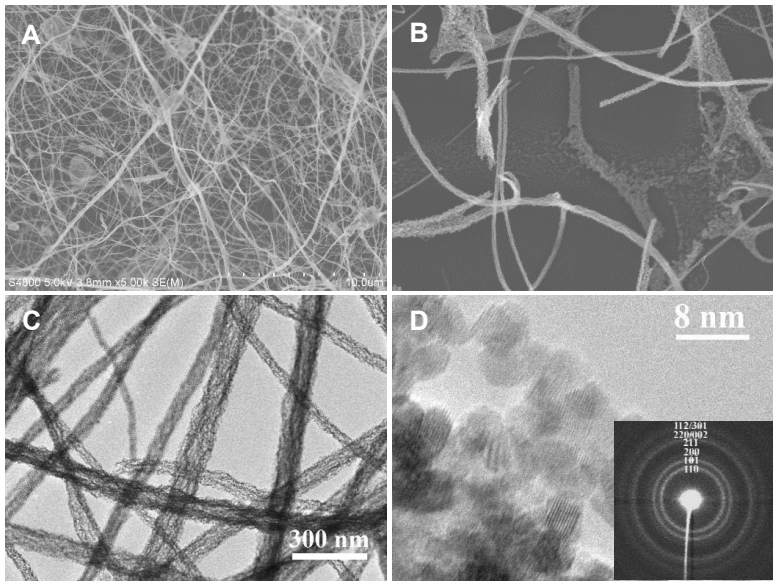

Figure 42 A) FESEM images of electrospun IrO_2 fibers after calcination at 500 °C, (B) Ir fibers obtained by H_2 treatment of the IrO_2 fibers, (C) and (D) TEM images from electrospun IrO_2 fibers. The insert in (D) is selected area electron diffraction (SAED) pattern from the same sample.

FESEM image (Figure 42) shows that the product after the calcination was in the form of fibers. XRD verified that these fibers were IrO_2. Diameters of these IrO_2 fibers were between 50 and 300 nm. TEM images demonstrated that the fibers consisted of nanoparticles which were about 5 nm in diameter. Selected area electron diffraction (SAED) confirmed that the fibers consisted of nanocrystalline IrO_2 (Figure 42D). XRD in Figure 43 verified that the fibers after the H_2 treatment were Ir. Both IrO_2 and Ir fibers were mechanically fragile.

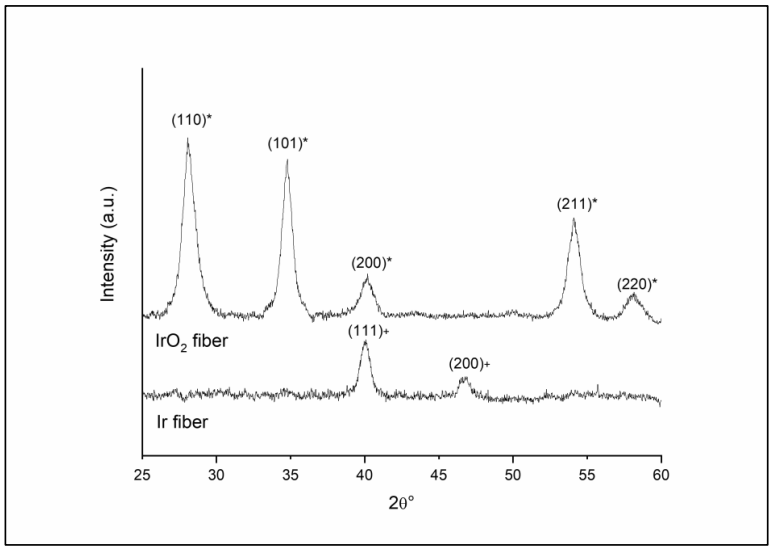

Figure 43 XRD from IrO_2 and Ir fibers. The indexes refer to metallic IrO_2 (+) and Ir (∗).

5.5.2 Ir and IrO_2 nanotubes by the TUFT process

Ir and IrO_2 nanotubes were prepared by depositing Ir and IrO_2 thin films on electrospun template PVP fibers by the $Ir(acac)_3/O_2$ and $Ir(acac)_3/O_3$ ALD processes, respectively after ALD, the coated fibers were calcined in air at 500 °C for 4 h.

The first attempt to prepare iridium nanotubes was to coat PVP fibers directly with Ir by using the ALD $Ir(acac)_3/O_2$ –process[133] at 225 °C. FESEM images revealed that this process failed. Iridium was deposited only on the supporting Si wafer on places not covered by PVP fibers (Figure 44). This observation indicated that PVP can passivate the surface against the Ir growth and soon after Färm et al. exploited this in making area-selective iridium ALD process.[134] The passivation effect of PVP could be avoided by coating the template fibers first with a few nanometers of ALD alumina seed layer. FESEM images showed that the template fibers with the alumina seed layer could be coated uniformly with iridium at 225 °C (Figure 45A). After calcination, SEM and XRD showed that the final product was Ir nanotube (Figures 45B and 47).

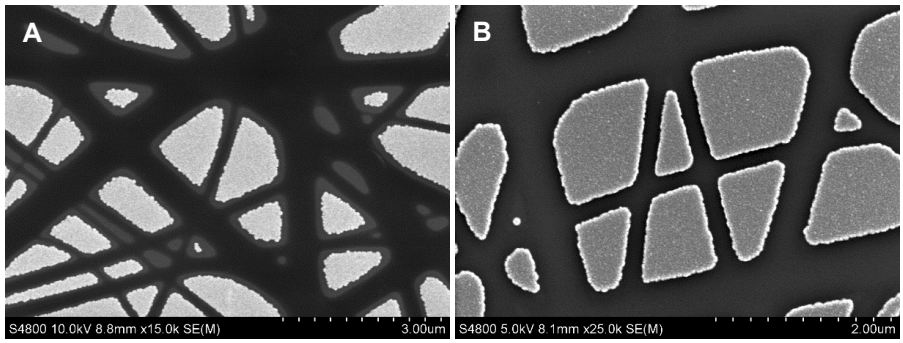

Figure 44 FESEM images of Ir films when deposition was attempted directly on PVP fibers on silicon (A) as deposited and (B) after calcination.

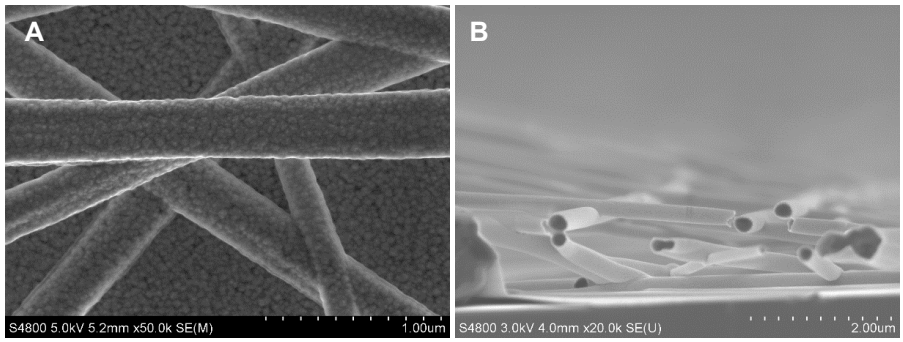

Figure 45 (A) FESEM images of PVP template fibers after ALD Al_2O_3 and Ir depositions at 225 °C. (B) Ir nanotubes obtained after calcination in air.

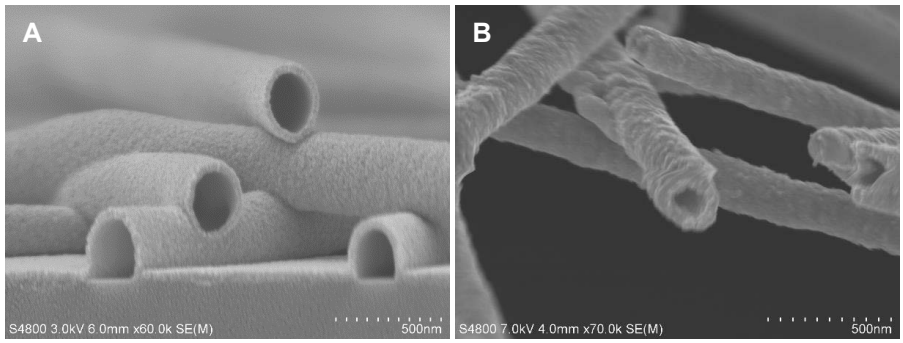

Figure 46 (A) FESEM image of IrO_2 tubes. (B) FESEM image of Ir tubes.

We also tried another ALD process[116] where the PVP fibers were coated using $Ir(acac)_3$ and O_3 at 165 °C. With this process IrO_2 thin films were deposited directly on the PVP fibers without the alumina seed layer (Figure 46). After the calcination, the final product was IrO_2 as verified by XRD (Figure 47).

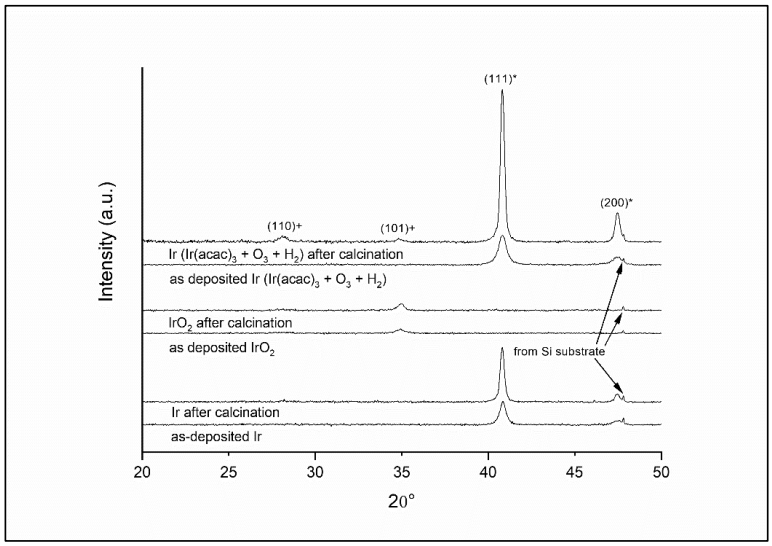

Figure 47 XRD from Ir and IrO_2 nanotubes. The indexes refer to metallic Ir (∗) and IrO_2 (+). Silicon was used as a supporting plate during the XRD measurement.

In addition, we tested an $Ir(acac)_3/O_3$ process that was modified by adding an H_2 pulse. The $Ir(acac)_3/O_3/H_2$ process[117] deposited at 165 °C iridium thin film directly on the PVP fibers. FESEM images after calcination showed that the tubular form was retained (Figure 46). XRD verified that the thin film was crystalline iridium, but there were also small reflections from the IrO_2 phase (Figure 47).

5.5.3 PtO_x and Pt nanotubes by TUFT process

PtO_x and Pt nanotubes were prepared by depositing PtO_x thin films on electrospun template fibers by the $Pt(acac)_2/O_3$ ALD process[118] at 120 °C. As-deposited thin films on PVP fibers were amorphous as verified by XRD and therefore most likely PtO_x in composition as known to be the product of this process[118] (Figure 49). Calcination at 500 °C removed the template PVP fibers and converted the PtO_x thin films to metallic Pt. FESEM images in Figure 48 show that the as-deposited PtO_x thin films on PVP fibers were smooth, but after the calcination the Pt tubes had porous surfaces with a pore size of about 50 nm or below. These pores are due to a large change of density during the

calcination. The density of PtO_x varies from 6 to 14 g/cm^3 while the density of Pt is 21 g/cm^3.

Part of the as-deposited PtO_x/PVP sample was treated with H_2 gas at room temperature. XRD verified that PtO_x was converted to crystalline metallic Pt. After calcination at 500 °C the H_2-treated sample was crystallized to the same level as obtained by calcining PtO_x directly. FESEM images showed that the reduction with H_2 gas at room temperature was too dramatic, because walls of the tubes were cracked along the fiber (Figure 48D and E).

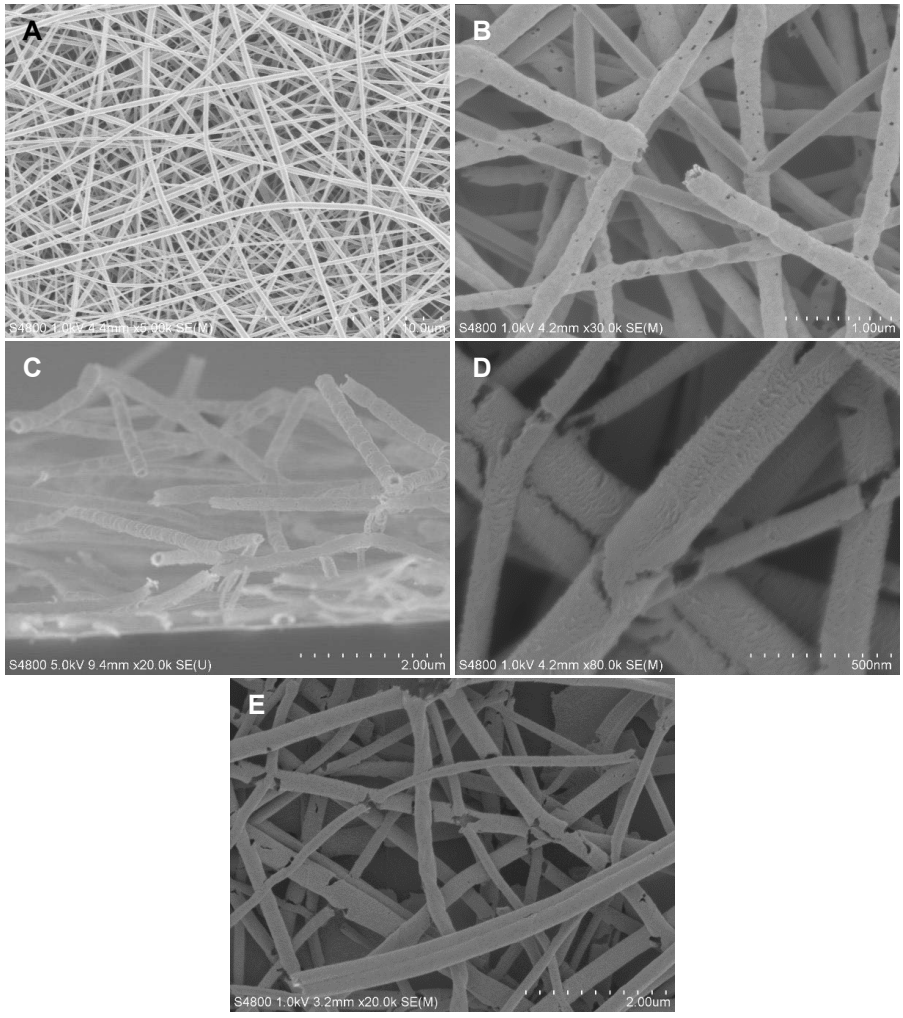

Figure 48 FESEM images of ALD PtO_x on PVP fiber template as-deposited (A) and after calcination in air (B and C). Pt fibers obtained by H_2 treatment of PtO_x coated PVP fibers before (D) and after (E) calcination.

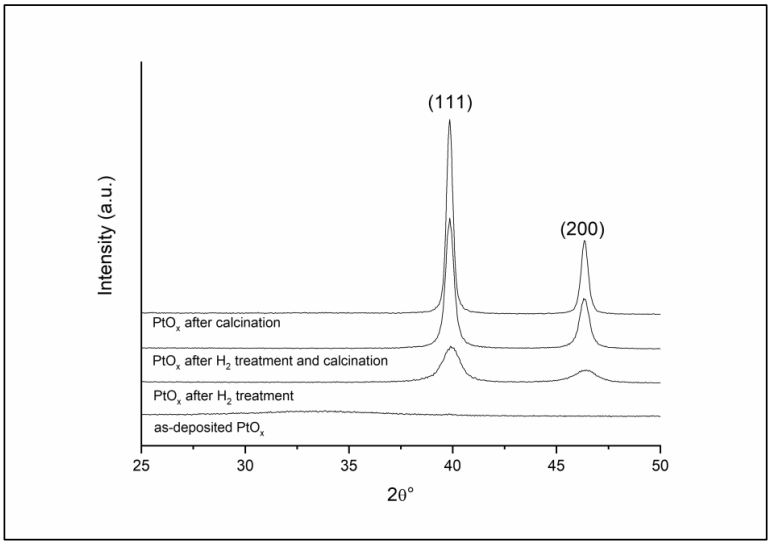

Figure 49 XRD of PtO_x and Pt tubes. The indexes refer to metallic Pt.

In conclusion, nanocrystalline IrO_2 fibers can be prepared by electrospinning $Ir(acac)_3$/PVP solution followed by calcination. The IrO_2 fibers are readily reduced to Ir fibers by hydrogen at room temperature. By combining the electrospinning and ALD methods in the TUFT process, it is possible to prepare iridium, platinum, IrO_2 and PtO_x nanotubes.

5.6 Sodium titanate fibers for water purification (V)

In this work, for the first time ever, inorganic metal oxide ion exchange fibers were prepared by electrospinning.[94,95] Inorganic ion exchange materials are extensively used in treating waste waters from e.g. nuclear power plants, where the concentration of the radioactive element can be extremely low compared to the total element concentration.[135] This is made possible by the high ion-exchange selectivity of these materials.[136-139] Selective inorganic ion-exchangers have been in a critical role in decontamination of radioactive solution e.g. from the Fukushima nuclear accident site.[140,141] These ion exchangers are typically used in a granulated form where the ion exchange rate is governed mainly by slow diffusion inside the granules.

This study presents an approach for improving the efficiency and sustainability of ion exchangers in the form of nanofibers. As compared to the granular ion-exchange materials, fibers have smaller dimensions. All ion exchange sites in the fibers are within a small diffusion length from the fiber surface, which enhances the kinetics of the ion exchange. Also, by preparing the material in the form of a fiber mat with a high surface area to volume ratio is considered ideal, because less mass is needed for a given capacity. The netlike macrostructure resists close packing and consequent clogging of the ion exchange column. From the environmental and end-user's viewpoints, electrospun ion exchange fibers provide highly efficient and sustainable material for separation of trace pollutants, such as radionuclides and other heavy metals from waste waters but also from contaminated fresh waters.

In this study we concentrated only on a sodium titanate ion exchange material. Sodium titanate is highly selective for strontium and one of the widely exploited inorganic ion exchange materials, and its commercial granular form, SrTreat® was readily available for reference.[138,139,141-143] As we already had a good electrospinning process for preparing bare TiO_2 fibers, it was straightforward to make sodium titanate fibers by just adding sodium into the TiO_2 electrospinning solution.[14]

Sodium titanate fibers were electrospun from a solution that contained proper amounts of sodium acetate, titanium(IV)isopropoxide, acetic acid, PVP and ethanol. Electrospinning was done with 15 kV voltage, 15 cm needle-collector distance, and 1.0 ml/h feed rate. Electrospun fibers were calcined at 500 °C for 4 h in air. The calcination temperature was selected based on the TGA measurement (Figure 50), because at 300-450 °C PVP is still combusting, and at 500 °C the mass decrease is essentially over. The shift in the combustion temperature of PVP from the bare PVP fibers to the composite fibers is notably large, nearly 150 °C.

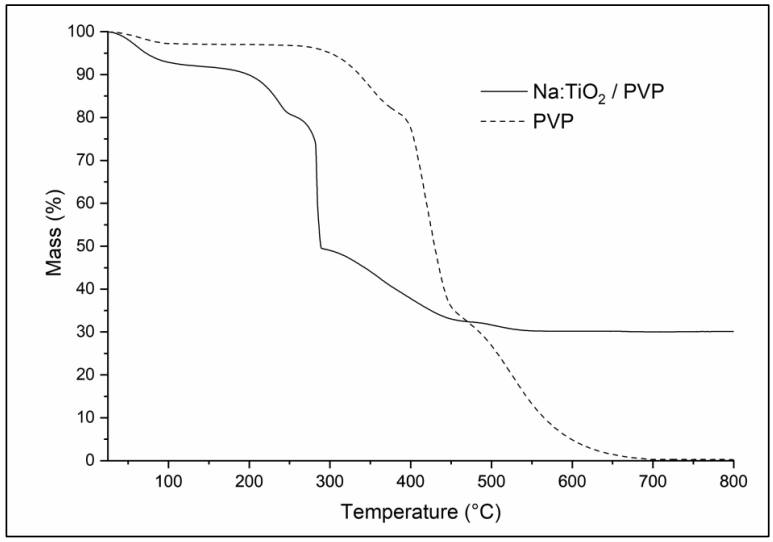

Figure 50 TGA measurement of the as-electrospun sodium titanate-PVP composite fibers (solid line), and, for comparison, as-electrospun PVP fibers (dashed line) heated with a rate of 10 °C/min in air. Reprinted from [V] by permission of Taylor & Francis, Copyright (2018).

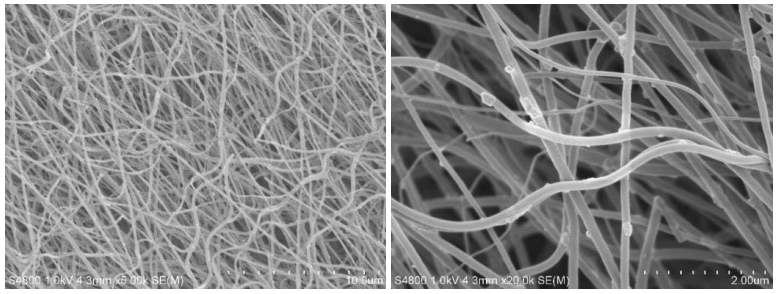

Figure 51 FESEM images with different magnifications of calcined electrospun sodium titanate fibers. Reprinted from [V] by permission of Taylor & Francis, Copyright (2018).

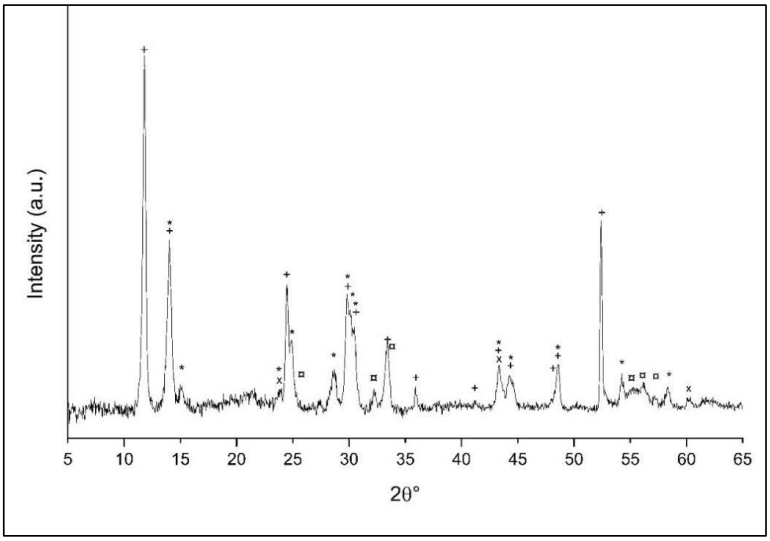

Figure 52 XRD pattern of electrospun sodium titanate fibers after calcination. The symbols refer to TiO_2 (*), $Na_2Ti_6O_{13}$ (+), $Na_2TiO_4 \cdot H_2O$ (¤) and Na_2O_2 (x). Reprinted from [V] by permission of Taylor & Francis, Copyright (2018).

FESEM images (Figure 51) show that the fibers exhibit smooth surfaces, and the average diameter after calcination was about 200 nm. XRD (Figure 52) verified that the fibers were mainly crystalline titanium dioxide (TiO_2) and monoclinic sodium titanate ($Na_2Ti_6O_{13}$).

Ion exchange properties of the electrospun fibers were studied by measuring their metal uptake capabilities using batch experiments.[V] The target ion in this study was strontium but cobalt was tested too because sodium titanate is known to be effective for cobalt as well.[144] As a comparison also the commercial ion exchange material SrTreat® (Fortum Corporation) was tested. The results from these batch experiments are presented here as distribution coefficients (K_d, ml/g) that reveal how the element of an interest is distributed between the initial sample solution and the solid material after one day equilibration time. K_d was calculated as follows:

$$(1) \qquad K_d = \frac{(c_i - c_{eq})}{c_{eq}} * \frac{V}{m}$$

Where c_i = initial metal concentration of the solution, c_{eq} = metal concentration of the solution at equilibrium, V = volume of the solution, and m = mass of the solid material. The concentrations of these trace ions were in ppt level or less than 10^{-15} mol/l.

Figure 53 shows that the synthesized sodium titanate fibers have good strontium uptake properties, and their cobalt uptake is also good when pH is below 7 and K_d is over 1000. The behavior of the fibers is similar to the granular material.[136,145] The K_d values increase with pH because two reactions compete simultaneously. In addition to the strontium and cobalt ion exchange reactions, the material tends to take also protons from the solution. When pH is increased, there are less protons available, which results in increased ion exchange reactions with the target ions. When pH is increased over 7 cobalt is hydrolyzed to $Co(OH)_2$ (aq), that as a neutral molecule is poorly taken up by the material. At this low concentrations $Co(OH)_2$ does not precipitate either.

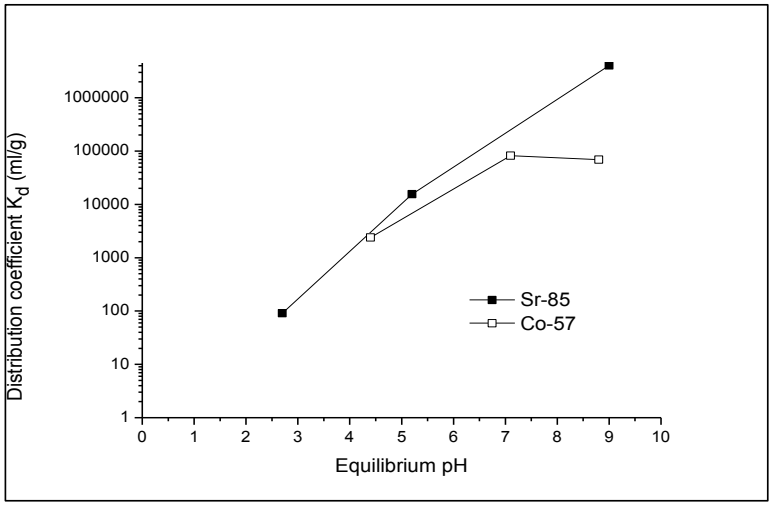

Figure 53 Distribution coefficients of Sr-85 and Co-57 in 0.1 M $NaNO_3$ solution as a function of pH for electrospun sodium titanate fibers. The initial concentration of Sr-85 and Co-57 were less than 10^{-15} mol/l. Reprinted from [V] by permission of Taylor & Francis, Copyright (2018).

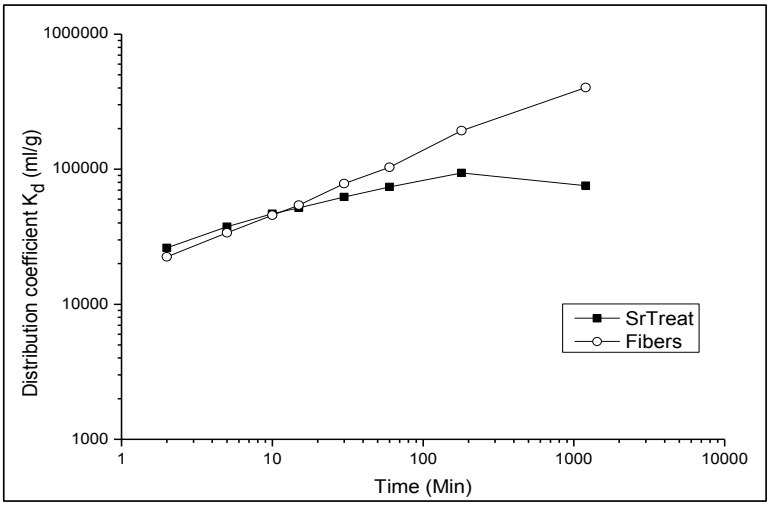

Figure 54 Distribution coefficient K_d (ml/g) of SrTreat® and calcined electrospun sodium titanate fibers as a function of time (pH = 6.5). Reprinted from [V] by permission of Taylor & Francis, Copyright (2018).

The kinetic ion exchange experiments in Figure 54 show that after the first two points (2 and 5 min) the fibrous material has higher distribution coefficients than the SrTreat®. While the uptake trend of the fibrous material keeps on increasing, the uptake trend of the granular material is already getting slower due to the longer diffusion lengths in the granular material. The last SrTreat® measurement point shows even a decrease. This may be because the magnetic stirring bar ground the SrTreat® granules to smaller and smaller pieces, and the smallest pieces were able to come through the filter used for sampling the liquid. This behavior is not seen with the fibers.

In conclusion, our study has proved that electrospun sodium titanate fibers can be used as an ion exchange material for strontium and cobalt ions. Strontium uptake properties are comparable or better to the commercial SrTreat® material. By exploiting electrospun inorganic fibers the mass of ion exchange material required for a given capacity can be decreased significantly. Later this approach has been extended to ZrO_2 fibers for removal of antimonates, Sb(V),[146] and further work on other ion exchange materials is on-going.

6 CONCLUSIONS

Electrospinning is a very versatile method to produce fibrous nanostructures. It can produce macroscopic amounts of nanofibers from several materials, for example inorganic fibers, synthetic polymer fibers, and fibers of natural materials. The method is relatively fast, and the apparatus can be simple and inexpensive.

ALD is a straightforward method to deposit conformal thin films with atomic layer accuracy. It can be used to change the surface composition and thereby the properties of electrospun fibers. The two methods together are ideal for making nanotubes by using electrospun fibers as templates and ALD for coating them in the TUFT process.

We built our own electrospinning setup and verified its operation. In addition, we successfully expanded the setup with various kinds of static and moving collectors. Needleless twisted wire electrospinning setup was developed and proved that electrospinning can be done also in a larger scale. The alignment of fibers was achieved at some level too.

In this study we successfully demonstrated that electrospinning and ALD can be used together to prepare inorganic nanotubes of Al_2O_3, TiO_2, Ir, IrO_2, Pt and PtO_x. Thin films grew on the template fibers smoothly and conformally, and both properties were retained after calcination. The materials selection can be largely extended because essentially all thermal ALD processes should be applicable with electrospun fibers.

We also succeeded for the first time in preparing metallic Ir and IrO_2 nanofibers by the electrospinning technique. This demonstrates how it could be possible to prepare fibers of also other noble metals and their oxides.

We also showed that by using a combination of electrospinning and ALD it is possible to prepare both solid core/sheath nanofibers and partly filled nanotubes depending on the order of calcination and ALD coating of electrospun fibers. This procedure is simple and versatile, and it allows to prepare various kinds of composite nanofibers and nanotubes.

Perhaps the most significant result of this study was the utilization of electrospun ion-selective sodium titanate nanofibers for purification of radioactive wastewaters as needed for example in the Fukushima powerplant accident site in much larger scale than before. This invention has already been patented and further development is ongoing. It may develop to an environmentally significant method for purifying waters around the world.

Because there are numerous known electrospinning and ALD processes and both methods are widely investigated, there are many possibilities to prepare various fibrous, tubular and their composite structures. Environmental exploitation of fibers has already been proven in this study. Next challenge and topic for further investigation is adoption of these tubes and fibers to real applications efficiently. Scale-up of the fiber synthesis is of the highest importance for this.

7 REFERENCES

[1] Bureau international des poids et mesures, *Le Système international d'unités - The International System of Units,* **(2006),** Bureau international des poids et mesures, France, Paris.

[2] B. Cordero, V. Gomez, A. E. Platero-Prats, M. Reves, J. Echeverria, E. Cremades, F. Barragan and S. Alvarez*, Dalton Trans.* **(2008)** 2832-2838.

[3] O. D. Velev, P. M. Tessier, A. M. Lenhoff and E. W. Kaler*, Nature* 401 **(1999)** 548.

[4] P. Mulvaney*, ACS Nano* 9 **(2015)** 2215-2217.

[5] M. Bognitzki, H. Hou, M. Ishaque, T. Frese, M. Hellwig, C. Schwarte, A. Schaper, J. H. Wendorff and A. Greiner*, Adv. Mater.* 12 **(2000)** 637-640.

[6] A. Formhals, **(1934)** US patent *1975504,*

[7] D. H. Reneker and A. L. Yarin*, Polymer* 49 **(2008)** 2387-2425.

[8] D. H. Reneker, A. L. Yarin, H. Fong and S. Koombhongse*, J. Appl. Phys.* 87 **(2000)** 4531-4547.

[9] D. H. Reneker and I. Chun*, Nanotechnology* 7 **(1996)** 216-223.

[10] A. Greiner and J. H. Wendorff, *Self-Assembled Nanomaterials I,* Vol 219, **(2008)** ed T Shimizu , Springer, Berlin / Heidelberg, Germany, pp. 107-171.

[11] A. Greiner and J. H. Wendorff*, Angew. Chem. Int. Ed.* 46 **(2007)** 5670-5703.

[12] D. Li, Y. Wang and Y. Xia*, Nano Lett.* 3 **(2003)** 1167-1171.

[13] D. Li, T. 1. Herricks and Y. Xia*, Appl. Phys. Lett.* 83 **(2003)** 4586-4588.

[14] D. Li and Y. Xia*, Nano Lett.* 3 **(2003)** 555-560.

[15] D. Li, Y. Wang and Y. Xia*, Adv. Mater.* 16 **(2004)** 361-366.

[16] D. Li and Y. Xia*, Nano Lett.* 4 **(2004)** 933-938.

[17] D. Li and Y. Xia*, Adv. Mater.* 16 **(2004)** 1151-1170.

[18] D. Li, J. T. McCann, M. Gratt and Y. Xia*, Chemical Physics Letters* 394 **(2004)** 387-391.

[19] D. Li, J. T. McCann and Y. Xia*, Small* 1 **(2005)** 83-86.

[20] D. Li, Y. H. Leung, A. B. Djurisic, Z. T. Liu, M. H. Xie, J. Gao and W. K. Chan*, Journal of Crystal Growth* 282 **(2005)** 105-111.

[21] D. Li, G. Ouyang, J. T. McCann and Y. Xia*, Nano Lett.* 5 **(2005)** 913-916.

[22] S. Ramakrishna, K. Fujihara, W. E. Teo, T. Lim and Z. Ma, *An introduction to Electrospinning and Nanofibers,* **(2005),** World Scientific, Singapore.

[23] S. Ramakrishna, K. Fujihara, W. Teo, T. Yong, Z. Ma and R. Ramaseshan*, Materials Today* 9 **(2006)** 40-50.

[24] R. Ramaseshan, S. Sundarrajan, R. Jose and S. Ramakrishna*, J. Appl. Phys.* 102 **(2007)** 111101.

[25] W. E. Teo, M. Kotaki, X. M. Mo and S. Ramakrishna*, Nanotechnology* **(2005)** 918-924.

[26] W. E. Teo and S. Ramakrishna*, Nanotechnology* 17 **(2006)** R89-R106.

[27] S. Tan, R. Inai, M. Kotaki and S. Ramakrishna*, Polymer* 46 **(2005)** 6128-6134.

[28] G. Taylor*, Proceedings of the Royal Society of London.Series A.Mathematical and Physical Sciences* 280 **(1964)** 383-397.

[29] S. L. Shenoy, W. D. Bates, H. L. Frisch and G. E. Wnek*, Polymer* 46 **(2005)** 3372-3384.

[30] H. Fong, I. Chun and D. H. Reneker*, Polymer* 40 **(1999)** 4585-4592.

[31] S. Megelski, J. S. Stephens, D. B. Chase and J. F. Rabolt*, Macromolecules* 35 **(2002)** 8456-8466.

[32] C. Mit-uppatham, M. Nithitanakul and P. Supaphol*, Macromol. Chem. Phys.* 205 **(2004)** 2327-2338.

[33] J. Kameoka, R. Orth, Y. Yang, D. Czaplewski, R. Mathers, G. W. Coates and H. G. Craighead*, Nanotechnology* 14 **(2003)** 1124-1129.

[34] X. Zong, K. Kim, D. Fang, S. Ran, B. S. Hsiao and B. Chu*, Polymer* 43 **(2002)** 4403-4412.

[35] J. Zeng, X. Xu, X. Chen, Q. Liang, X. Bian, L. Yang and X. Jing*, J. Controlled Release* 92 **(2003)** 227-231.

[36] C. J. Angammana and S. H. Jayaram*, IEEE Transactions on Industry Applications* 47 **(2011)** 1109-1117.

[37] W. K. Son, J. H. Youk, T. S. Lee and W. H. Park*, Polymer* 45 **(2004)** 2959-2966.

[38] C. Hsu and S. Shivkumar*, Macromol. Mater. Eng* 289 **(2004)** 334-340.

[39] C. J. Buchko, L. C. Chen, Y. Shen and D. C. Martin*, Polymer* 40 **(1999)** 7397-7407.

[40] J. S. Lee, K. H. Choi, H. D. Ghim, S. S. Kim, D. H. Chun, H. Y. Kim and W. S. Lyoo*, J. Appl. Polym. Sci.* 93 **(2004)** 1638-1646.

[41] K. J. Pawlowski, H. L. Belvin, D. L. Raney, J. Su, J. S. Harrison and E. J. Siochi*, Polymer* 44 **(2003)** 1309-1314.

[42] S. Zhao, X. Wu, L. Wang and Y. Huang*, J. Appl. Polym. Sci.* 91 **(2004)** 242-246.

[43] G. C. Rutledge, Y. Li, S. V. Fridrikh, S. B. Warner, V. E. Kalayci and P. Patra*, National Textile Center Annual Report M01-D22* M01-D22 **(2001)** 1-10.

[44] M. M. Demir, I. Yilgor, E. Yilgor and B. Erman*, Polymer* 43 **(2002)** 3303-3309.

[45] R. Kessick and G. Tepper*, Appl. Phys. Lett.* 84 **(2004)** 4807-4809.

[46] D. Zhang and J. Chang*, Nano Lett.* 8 **(2008)** 3283-3287.

[47] P. Katta, M. Alessandro, R. D. Ramsier and G. G. Chase*, Nano Lett.* 4 **(2004)** 2215-2218.

[48] J. Ayutsede, M. Gandhi, S. Sukigara, M. Micklus, H. Chen and F. Ko*, Polymer* 46 **(2005)** 1625-1634.

[49] X. Yuan, Y. Zhang, C. Dong and J. Sheng*, Polym. Int.* 53 **(2004)** 1704-1710.

[50] A. Varesano, R. A. Carletto and G. Mazzuchetti*, J. Mater. Process. Technol.* 209 **(2009)** 5178-5185.

[51] S. A. Theron, A. L. Yarin, E. Zussman and E. Kroll*, Polymer* 46 **(2005)** 2889-2899.

[52] O. O. Dosunmu, G. G. Chase, W. Kataphinan and D. H. Reneker, *Nanotechnology* 17 **(2006)** 1123-1127.

[53] J. S. Varabhas, G. G. Chase and D. H. Reneker, *Polymer* 49 **(2008)** 4226-4229.

[54] B. Ding, E. Kimura, T. Sato, S. Fujita and S. Shiratori, *Polymer* 45 **(2004)** 1895-1902.

[55] J. M. Deitzel, J. Kleinmeyer, D. Harris and N. C. Beck Tan, *Polymer* 42 **(2001)** 261-272.

[56] L. Wannatong, A. Sirivat and P. Supaphol, *Polym. Int.* 53 **(2004)** 1851-1859.

[57] C. L. Casper, J. S. Stephens, N. G. Tassi, D. B. Chase and J. F. Rabolt, *Macromolecules* 37 **(2004)** 573-578.

[58] P. K. Baumgarten, *J. Colloid. Interface Sci.* 36 **(1971)**

[59] Z. Huang, Y. -. Zhang, M. Kotaki and S. Ramakrishna, *Compos. Sci. Technol.* 63 **(2003)** 2223-2253.

[60] C. Lin, T. Tsai, M. Chung and S. Lu, *J. Appl. Phys.* 105 **(2009)** 07B509.

[61] D. M. Bigg, *Composites* 10 **(1979)** 95-100.

[62] J. Y. Li, Y. Sun, Y. Tan, F. M. Xu, X. L. Shi and N. Ren, *Chem. Eng. J.* 144 **(2008)** 149-152.

[63] Y. Qiu, J. Yu, J. Rafique, J. Yin, X. Bai and E. Wang, *J. Phys. Chem. C* 113 **(2009)** 11228-11234.

[64] Y. Sun, J. Y. Li, Y. Tan and L. Zhang, *J. Alloys Compounds* 471 **(2009)** 400-403.

[65] H. Wu, Y. Sun, D. Lin, R. Zhang, C. Zhang and W. Pan, *Adv. Mater.* 21 **(2009)** 227-231.

[66] B. Eick and J. Youngblood, *J. Mater. Sci.* 44 **(2009)** 160-165.

[67] X. M. Cui, Y. S. Nam, J. Y. Lee and W. H. Park, *Mater. Lett.* 62 **(2008)** 1961-1964.

[68] P. Zhu, Y. Hong, B. Liu and G. Zou, *Nanotechnology* 20 **(2009)** 255603 (6pp).

[69] Y. Wu, H. Larry L., D. Jing, C. Kwan-leong and G. Jingkun*, J. Am. Ceram. Soc.* 87 **(2004)** 1988-1991.

[70] L. Chunmei, J. Hyoung-Joon, B. Gregory D. and K. David L.*, J. Mater. Res.* 20 **(2005)** 3374-3384.

[71] H. Kim and H. Kim*, Journal of Biomedical Materials Research Part B: Applied Biomaterials* 77B **(2006)** 323-328.

[72] V. Pore, A. Rahtu, M. Leskelä, M. Ritala, T. Sajavaara and J. Keinonen*, Chem. Vap. Deposition* 10 **(2004)** 143-148.

[73] J. H. Yin, J. Ding, J. S. Chen and X. S. Miao*, J. Magn. Magn. Mater.* 303 **(2006)** e387-e391.

[74] G. Sarala Devi, V. Bala Subrahmanyam, S. C. Gadkari and S. K. Gupta*, Anal. Chim. Acta* 568 **(2006)** 41-46.

[75] W. S. Rees, *CVD of Nonmetals,* **(1996),** VCH, Weinheim.

[76] T. Asikainen, M. Ritala and M. Leskelä*, J. Electrochem. Soc.* 142 **(1995)** 3538-3541.

[77] Y. Chen, C. Lee, M. Yeng and H. Chiu*, J. Cryst. Growth* 247 **(2003)** 363-370.

[78] C. Sung-Seen, G. L. Seung, S. I. Seung, H. K. Seong and Y. L. Joo*, J. Mater. Sci. Lett.* 22 **(2003)** 891-893.

[79] J. Shui and J. C. M. Li*, Nano Lett.* 9 **(2009)** 1307-1314.

[80] H. J. Kim, Y. S. Kim, M. H. Seo, S. M. Choi and W. B. Kim*, Electrochem. Commun.* 11 **(2009)** 446-449.

[81] Y. S. Kim, S. H. Nam, H. Shim, H. Ahn, M. Anand and W. B. Kim*, Electrochem. Commun.* 10 **(2008)** 1016-1019.

[82] V. G. Pol, E. Koren and A. Zaban*, Chem. Mater.* 20 **(2008)** 3055-3062.

[83] G. Y. Han, B. Guo, L. W. Zhang and B. S. Yang*, Adv. Mater.* 18 **(2006)** 1709-1712.

[84] M. Bognitzki, M. Becker, M. Graeser, W. Massa, J. H. Wendorff, A. Schaper, D. Weber, A. Beyer, A. Gölzhäuser and A. Greiner*, Adv. Mater.* 18 **(2006)** 2384-2386.

[85] S. Agarwal, A. Greiner and J. H. Wendorff*, Adv. Funct. Mater.* 19 **(2009)** 2863-2879.

[86] E. Kostakova, L. Meszaros and J. Gregr*, Mater. Lett.* 63 **(2009)** 2419-2422.

[87] H. He, C. Liu and K. Molnar*, Fibers and Polymers* 19 **(2018)** 1472-1478.

[88] S. Agarwal, A. Greiner and J. H. Wendorff*, Chemie Ingenieur Technik* 80 **(2008)** 1671-1676.

[89] D. Petras, M. Maly, M. Kovac, V. Stromsky, J. Pozner, J. Trdlicka, L. Mares, J. Cmelik and F. Jakubek, **(2009)** PCT Int. Appl. *WO2009010020*, 45pp.

[90] J. B. Chiu, Y. K. Luu, D. Fang, B. S. Hsiao, B. Chu and M. Hadjiargyrou*, Journal of Biomedical Nanotechnology* 1 **(2005)** 115-132.

[91] J. E. Armantrout, M. A. Bryner, M. C. Davis and Y. M. Kim, **(2006)** U.S. Pat. Appl. Publ. *US20060012084A1,* 9 pp.

[92] J. E. Armantrout, M. A. Bryner and C. B. Spiers, **(2009)** U.S. Patent *US7582247B2,* 9pp.

[93] J. Holopainen **(2017),** *Bioactive Coatings and Fibers for Bone Implants and Scaffolds by Atomic Layer Deposition, Electrospinning, Solution Blow Spinning and Electroblowing.* Academic Dissertation, University of Helsinki.

[94] R. Harjula, R. Koivula, M. Ritala, E. Santala, J. Holopainen and E. Tusa, **(2018)** PCT Int. Appl. *WO2018215696A1,* 40pp.

[95] E. Tusa, R. Harjula, R. Koivula, M. Ritala, E. Santala and J. Holopainen, **(2019)** Finnish Patent *FI127747B,* 40pp.

[96] T. Suntola*, Thin Solid Films* 216 **(1992)** 84-89.

[97] M. Ritala and M. Leskelä, *Handbook of Thin Film Materials,* Vol 1, **(2001)** ed H S Nalwa , Academic Press, San Diego, CA, pp. 103-159.

[98] R. L. Puurunen*, J. Appl. Phys.* 97 **(2005)** 121301.

[99] V. Miikkulainen, M. Leskelä, M. Ritala and R. L. Puurunen*, J. Appl. Phys.* 113 **(2013)** 021301.

[100] H. C. M. Knoops, S. E. Potts, A. A. Bol and W. M. M. Kessels, *Handbook of Crystal Growth,* **(2015)** ed T F Kuech , Elsevier, pp. 1101-1134.

[101] M. Ritala and M. Leskelä, *Handbook of Thin Films,* **(2002)** ed H Singh Nalwa , Academic Press, Burlington, pp. 103-159.

[102] ALD database, https://www.atomiclimits.com/alddatabase/, *DOI: 10.6100/alddatabase,* Accessed: 24.8.2019 .

[103] J. Yuh, J. C. Nino and W. M. Sigmund*, Mater. Lett.* 59 **(2005)** 3645-3647.

[104] J. Yuh, L. Perez, W. M. Sigmund and J. C. Nino*, Physica E* 37 **(2007)** 254-259.

[105] Y. Zhang, X. He, J. Li, Z. Miao and F. Huang*, Sens. Actuator B-Chem.* 132 **(2008)** 67-73.

[106] D. Lin, H. Wu, R. Zhang and W. Pan*, J. Am. Ceram. Soc.* 90 **(2007)** 3664-3666.

[107] A. Azad*, Mater. Sci. Eng. A* 435-436 **(2006)** 468-473.

[108] Y. Zhu, J. C. Zhang, J. Zhai and L. Jiang*, Thin Solid Films* 510 **(2006)** 271-274.

[109] N. Dharmaraj, C. H. Kim, K. W. Kim, H. Y. Kim and E. K. Suh*, Spectrochim. Acta A Mol. Biomol. Spectrosc.* 64 **(2006)** 136-140.

[110] S. Piperno, L. Lozzi, R. Rastelli, M. Passacantando and S. Santucci*, Appl. Surf. Sci.* 252 **(2006)** 5583-5586.

[111] H. Dong, V. Nyame, A. G. MacDiarmid and W. E. Jones Jr.*, J. Polym. Sci. Part B: Polym. Phys.* 42 **(2004)** 3934-3942.

[112] K. Ohkawa, D. Cha, H. Kim, A. Nishida and H. Yamamoto*, Macromol. Rapid Commun.* 25 **(2004)** 1600-1605.

[113] Q. Peng, X. -. Sun, J. C. Spagnola, G. K. Hyde, R. J. Spontak and G. N. Parsons*, Nano Lett.* 7 **(2007)** 719-722.

[114] M. Ritala, M. Leskelä, E. Nykanen, P. Soininen and L. Niinisto*, Thin Solid Films* 225 **(1993)** 288-295.

[115] T. Aaltonen, M. Ritala, Y. Tung, Y. Chi, K. Arstila, K. Meinander and M. Leskelä*, J. Mater. Res.* 19 **(2004)** 3353-3358.

[116] J. Hämäläinen, M. Kemell, F. Munnik, U. Kreissig, M. Ritala and M. Leskelä*, Chem. Mater.* 20 **(2008)** 2903-2907.

[117] J. Hämäläinen, E. Puukilainen, M. Kemell, L. Costelle, M. Ritala and M. Leskelä*, Chem. Mater.* 21 **(2009)** 4868-4872.

[118] J. Hämäläinen, F. Munnik, M. Ritala and M. Leskelä*, Chem. Mater.* 20 **(2008)** 6840-6846.

[119] R. Kessick and G. Tepper, *Sens. Actuator B-Chem.* 117 **(2006)** 205-210.

[120] H. Niu, *Nanofibers,* **(2011)** ed Xungai Wang , IntechOpen, Rijeka, pp. Ch. 2.

[121] B. Lu, Y. Wang, Y. Liu, H. Duan, J. Zhou, Z. Zhang, Y. Wang, X. Li, W. Wang, W. Lan and E. Xie, *Small* 6 **(2010)** 1612-1616.

[122] H. Niu, X. Wang and T. Lin, *The Journal of The Textile Institute* 103 **(2012)** 787-794.

[123] O. Jirsak, F. Sanetrnik, D. Lukas, V. Kotek, L. Martinova and J. Chaloupek, **(2004)** PCT Int. Appl. *WO2005024101*, 13 pp.

[124] K. M. Forward and G. C. Rutledge, *Chemical Engineering Journal* 183 **(2012)** 492-503.

[125] D. Lukas, A. Sarkar and P. Pokorny, *J. Appl. Phys.* 103 **(2008)** 084309.

[126] A. L. Yarin and E. Zussman, *Polymer* 45 **(2004)** 2977-2980.

[127] N. M. Thoppey, J. R. Bochinski, L. I. Clarke and R. E. Gorga, *Polymer* 51 **(2010)** 4928-4936.

[128] X. Wang, H. Niu, T. Lin and X. Wang, *Polym. Eng. Sci.* 49 **(2009)** 1582-1586.

[129] E. Santala, M. Kemell, T. Pilvi, M. Ritala and M. Leskelä , *Inorganic nanotubes via electrospinning and ALD,* **(2006)** Oslo, Norway The Baltic conference on Atomic Layer Deposition, The Baltic conference on Atomic Layer Deposition, P3.

[130] G. -. Kim, S. -. Lee, G. H. Michler, H. Roggendorf, U. Gösele and M. Knez, *Chem. Mater.* 20 **(2008)** 3085-3091.

[131] J. Ahn, C. Ahn, S. Jeon and J. Park, *Applied Sciences* 9 **(2019)**

[132] Y. Ju, J. Park, H. Jung, S. Cho and W. Lee, *Mater. Sci. Eng. B* 147 **(2008)** 7-12.

[133] T. Aaltonen, M. Ritala, V. Sammelselg and M. Leskelä, *J. Electrochem. Soc.* 151 **(2004)** G489-G492.

[134] E. Färm, M. Kemell, E. Santala, M. Ritala and M. Leskelä, *J. Electrochem. Soc.* 157 **(2010)** K10-K14.

[135] J. Lehto, *Spec. Publ. - R. Soc. Chem.* 122 **(1993)** 39-53.

[136] J. Lehto, L. Brodkin, R. Harjula and E. Tusa*, Nucl. Technol.* 127 **(1999)** 81-87.

[137] J. Lehto, L. Brodkin, R. Harjula and E. Tusa , *SrTreat - a highly effective ion exchanger for the removal of radioactive strontium from nuclear waste solutions,* **(1997)** Singapore 6th, Proceedings of the International Conference on Radioactive Waste Management and Environmental Remediation, Proc. Int. Conf. Radioact. Waste Manage. Environ. Rem., 6th, 245-248.

[138] D. Alby, C. Charnay, M. Heran, B. Prelot and J. Zajac*, Journal of Hazardous Materials* 344 **(2018)** 511-530.

[139] W. He, K. Ai, X. Ren, S. Wang and L. Lu*, J. Mater. Chem. A* 5 **(2017)** 19593-19606.

[140] J. Lehto, R. Koivula, H. Leinonen, E. Tusa and R. Harjula*, Separation & Purification Reviews* **(2019)** 1-21.

[141] E. Tusa , *Cesium and Strontium Removal with Highly Selective Ion Exchange Media in Fukushima and Cesium Removal with Less Selective Media,* **(2014)** Phoenix, Arizona, USA 40th, The annual Waste Management Conference Proceedings, 14018.

[142] Y. Ishikawa, S. Tsukimoto, K. S. Nakayama and N. Asao*, Nano Lett.* 15 **(2015)** 2980-2984.

[143] L. Nian, Z. Lide, C. Yongzhou, F. Ming, Z. Junxi and W. Huimin*, Adv. Funct. Mater.* 22 **(2012)** 835-841.

[144] V. d. A. Cardoso, A. G. d. Souza, P. P. C. Sartoratto and L. M. Nunes*, Colloids Surf., A* 248 **(2004)** 145-149.

[145] J. Lehto, R. Harjula and A. Girard*, J. Chem. Soc., Dalton Trans.* **(1989)** 101-103.

[146] S. Lönnrot, V. Suorsa, J. Paajanen, T. Hatanpää, M. Ritala and R. Koivula*, RSC Adv.* 9 **(2019)** 22355-22365.